

Modern trends in Superconductivity and Superfluidity

Selected Chapters.

M.Yu. Kagan
P.L. Kapitza Institute for Physical Problems
kagan@kapitza.ras.ru

In preparation for Springer-Verlag

Chapter 11. Superconductivity in the low-density electron systems with repulsion.

Content

- 11.1. Kohn-Luttinger mechanism of SC in purely repulsive Fermi-systems.
- 11.2. Unconventional (anomalous) superconductive materials.
- 11.3. 3D and 2D Fermi-gas with repulsion. Triplet p-wave pairing.
 - 11.3.1. 3D Fermi-gas with repulsion.
 - 11.3.2. Triplet p-wave pairing.
 - 11.3.3. Model-independent considerations of Prof. P.Nozieres.
 - 11.3.4. Two-dimensional case.
- 11.4. SC in 3D and 2D Hubbard model with repulsion at low electron density.
 - 11.4.1. 3D Hubbard model at low density.
 - 11.4.2. 2D Hubbard model.
 - 11.4.3. Qualitative phase-diagram at low density in 2D.
 - 11.4.4. SC in 2D Hubbard model at larger electron densities $n_{\text{el}} \leq 1$.
 - 11.4.5. Parquette solution at weak-coupling and close to half-filling.
- 11.5. SC in the jelly model for Coulomb electron plasma.
 - 11.5.1. Cascade of SC-transitions in the dense electron plasma.
 - 11.5.2. The dilute electron plasma.
- 11.6. SC and phase separation in Shubin-Vonsovsky model.
 - 11.6.1. Shubin-Vonsovsky model. p-wave SC at low density.
 - 11.6.2. Localization and phase separation in Shubin-Vonsovsky model at larger densities.
- 11.11. Reference list.

11.1. Kohn-Luttinger mechanism of SC in purely repulsive Fermi-systems.

The modern physics of superconductivity (SC) is a very rapidly progressing field of condensed-matter physics where the colossal intellectual efforts of the researchers are concentrated and the new knowledge is accumulated very intensively giving rise to the development of neighboring areas of physics, chemistry, material science and engineering.

The latest progress in this area during last 25 years of experimental and theoretical research in connected with the physics of high- T_C superconductivity in cuprates and other related materials such as plumbates-bismithates, magnesium diborides, superconductors based on FeAs and so on.

One of the most essential and unresolved question in this area connected with the mechanism of superconducting pairing: whether it is of electron-phonon origin as in standard BCS-like [30] superconductors such as Hg, Pb, Nb, Al, or is due to electron-electron interaction as in new unconventional superconductive systems such as ruthenates, organic superconductors, heavy-fermion compounds and so on.

In this chapter we will advocate non-phonon mechanism of superconductivity based on electron-electron interaction. Here according to Prof. P.W. Anderson [11.1] there are two basic questions:

- 1) to convert the sign of the Coulomb interaction
- 2) to understand the properties of the normal state in high- T_C materials and other unconventional SC-systems.

We agree with these statements. We will address them in Galitskii-Bloom [11.2, 11.3] Fermi-gas approach for low density electron systems. We will prove the existence of SC at low-density limit, in purely repulsive Fermi-systems where we are far from antiferromagnetic (AFM) and structural instabilities. Moreover in this limit we can develop a regular perturbation theory.

The small parameter of the problem is gas-parameter:

$$|a|p_F \ll 1; \hbar = 1, \quad (11.1.1)$$

where a – is the s-wave scattering length, p_F – is Fermi-momentum. Critical temperatures (T_C -s) which we obtain are not very low. Our theory often “works” even for rather high densities because of intrinsic nature of SC-instability. Our philosophy throughout this chapter is to solve exactly low-density limit and then go to higher densities. The basic mechanism which we address here is enhanced Kohn-Luttinger mechanism of SC. We will also check the normal state of low-density electron systems with respect to marginality [11.5].

11.2. Unconventional superconductive systems.

During last 30 years there is a huge progress in experimental and theoretical investigation of unconventional (anomalous) superconductive systems. Among the new materials with anomalous superconductive pairing there are examples of triplet p-wave ($S_{\text{tot}} = l = 1$) and singlet d-wave ($S_{\text{tot}} = 0; l = 2$) superconductors as well as multiband s-wave SC-systems ($S = l = 0$).

The p-wave SC with orbital momenta of the Cooper pair $l = 1$ and total spin of the pair $S_{\text{tot}} = 1$ is realized in:

- fermionic isotopes of alkali elements ^6Li and ^{40}K in magnetic traps in the regime of Feshbach resonance at ultralow temperatures $T_C \sim (10^{-6} \div 10^{-7})$ K [11.8, 11.9]
- superfluid A and B phases of ^3He at very low critical temperatures $T_C \sim 1$ mK [11.6, 11.7]
- heavy-fermion superconductors $\text{U}_{1-x}\text{Th}_x\text{Be}_{13}$, UNi_2Al_3 , $T_C \sim (0.5 \div 1)$ K, heavy electron mass $m^* \sim (100 \div 200)m_e$ due to strong correlations [11.10]
- ruthenates Sr_2RuO_4 , $T_C \sim 1$ K (part of the community assumes d-wave pairing in these materials) [11.12]
- organic superconductor $\alpha\text{-(BEDT-TTF)}_2\text{I}_3$, $T_C \sim 5$ K [11.11].

Singlet d-wave pairing is realized in:

- heavy-fermion SC UPt_3 , $T_C \sim 0.5$ K, large effective mass $m^* \sim 200 m_e$
- high- T_C superconductors [11.13] $\text{La}_{2-x}\text{Sr}_x\text{CuO}_4$, $\text{YBa}_2\text{Cu}_3\text{O}_{7-\delta}$, $\text{Bi}_2\text{Sr}_2\text{Ca}_2\text{Cu}_3\text{O}_{10}$, $\text{Tl}_2\text{Sr}_2\text{Ca}_2\text{Cu}_3\text{O}_{10}$, $\text{Hg}_2\text{Ba}_2\text{Ca}_2\text{Cu}_3\text{O}_{10}$.

In all the families of high- T_C materials the elementary block CuO is present. They are called cuprates. T_C -s are in the range from 36 K for lanthanum-based family to 160 K for Hg-based family under pressure (the record established T_C in cuprates for today). Note that part of the community still assumes standard s-wave pairing in cuprates.

The highest T_C in unconventional SC corresponds to neutron stars which consist of 98% of bineutrons and 2% of biprotons. For bineutrons $S_{\text{tot}} = l = 1$, but there is a strong spin-orbit

coupling. So the total rotating moment $J = |\vec{S}_{tot} + \vec{l}| = 2$. According to theoretical predictions $T_C \sim (10^8 \div 10^{10})$ K for neutron stars.

Finally in the end of this section we would like to mention several unconventional SC systems of the multiband character with s-wave pairing, namely MgB_2 [11.14] (very promising for technical applications in electronics and energetics), and recently discovered family on the basis of FeAs such as $\text{BaFe}_2(\text{As}_{1-x}\text{P}_x)_2$ (with the coexistence of ferromagnetic fluctuations and SC) [11.15]. Note that part of the experimental community still hopes to demonstrate p-wave or d-wave SC in FeAs-based compounds [11.14c].

11.3. 3D and 2D Fermi-gas with repulsion. Triplet p-wave pairing.

The basic model to study non-phonon mechanism of SC in low density electron systems is a Fermi-gas model. In Fermi-gas with attraction s-wave scattering length $a < 0$ and we have unconventional s-wave pairing ($S = l = 0$) with a critical temperature:

$$T_{CO} \approx 0.28 \varepsilon_F e^{\frac{\pi}{2|a|p_F}} \quad (11.3.1)$$

This result was obtained by Gor'kov and Melik-Barhudarov [11.16] soon after the appearance of a famous BCS-theory [11.0] and differs from the BCS-result in preexponential factor $0.28\varepsilon_F$ (instead of Debye-frequency ω_D in the phonon models typical for unconventional SC systems).

11.3.1. 3D Fermi-gas with repulsion.

In Fermi-gas with repulsion $a > 0$ – repulsive interaction of two particles in vacuum. We will show that for the effective interaction of two particles in substance (via polarization of a fermionic background) we can convert the sign of the interaction in the triplet p-wave channel (for $S_{tot} = l = 1$) and get:

$$T_{C1} \sim \varepsilon_F e^{\frac{1}{(ap_F)^2}}, \quad (11.3.2)$$

where $\varepsilon_F = p_F^2/2m$ is Fermi-energy. This highly nontrivial result was obtained by Fay, Laser [11.17] and Kagan, Chubukov [11.18]. The most important is to understand what is effective interaction U_{eff} ? We will show that in momentum space in first two orders of the gas-parameter (11.1.1):

$$U_{eff}(\vec{p}, \vec{k}) = \frac{4\pi a}{m} + \left(\frac{4\pi a}{m} \right)^2 \Pi(\vec{p} + \vec{k}) \quad (11.3.3)$$

where $\Pi(\vec{p} + \vec{k})$ is a static polarization operator. It is given by a standard formula [11.19, 11.20]:

$$\Pi(q) = \int \frac{d^3 \vec{p}}{(2\pi)^3} \frac{n_F(\varepsilon_{p+q}) - n_F(\varepsilon_p)}{(\varepsilon_p - \varepsilon_{p+q})} \quad (11.3.4)$$

where $\varepsilon_p = \frac{p^2}{2m}$; $\varepsilon_{p+q} = \frac{(\vec{p} + \vec{q})^2}{2m}$ are the energy spectra and $n_F(\varepsilon_p) = \frac{1}{(e^{\varepsilon_p/T} + 1)}$, $n_F(\varepsilon_{p+q})$ are

Fermi-Dirac distribution functions. At low temperatures $T \ll \varepsilon_F$ polarization operator besides a regular part contains a Kohn's anomaly [11.21] of the form:

$$\Pi_{sing}(q) \sim (q - 2p_F) \ln|q - 2p_F| \quad \text{in 3D} \quad (11.3.5)$$

In real space Kohn's anomaly leads to Friedel oscillations (RKKY interaction) [11.22]. For dimensionless product of U_{eff} and 3D density of states:

$$N_{3D}(0) = \frac{mp_F}{2\pi^2} \quad (11.3.6)$$

we have in real space (see Fig. 11.1.):

$$N_{3D}(0)U_{\text{eff}}(r) \sim (ap_F)^2 \frac{\cos(2p_F r)}{(2p_F r)^3} \quad (11.3.7)$$

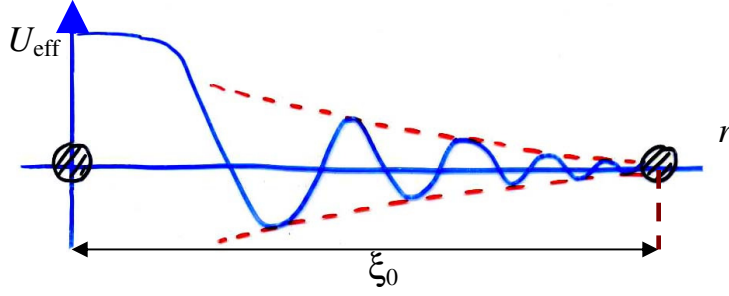


Fig. 11.1. Friedel oscillations in the effective interaction of two particles via polarization of a fermionic background. ξ_0 is a coherence length of a Cooper pair.

Thus we start from pure hard-core repulsion in vacuum and get the competition between repulsion and attraction in substance.

It is possible to show [11.4] that a singular part of U_{eff} “plays” in favor of attraction for large orbital momenta $l \gg 1$, while a regular part of U_{eff} – in favor of repulsion. Standard s-wave pairing is suppressed by hard-core repulsion. However as it was shown in [11.17, 11.18] the Kohn-Luttinger effect can be extended from the large momenta $l \gg 1$ to $l = 1$ and the attractive contribution is dominant even for p-wave channel. The exact solution [11.17, 11.18] yields for the critical temperature:

$$T_{C1} \sim \varepsilon_F e^{\frac{5\pi^2}{4(2\ln 2 - 1)(ap_F)^2}} \quad (11.3.8)$$

11.3.2. Triplet p-wave pairing.

Note that diagrammatically effective interaction U_{eff} corresponds to the irreducible bare vertex and is given by the set of diagrams which cannot be separated by two lines running in the same direction [11.19, 11.20] (thus U_{eff} does not contain the Cooper loop). Correspondingly the formula (11.3.3) can be represented as:

$$U_{\text{eff}}(\vec{p}, \vec{k}) = \frac{4\pi a}{m} + \left(\frac{4\pi a}{m} \right)^2 \Phi(\vec{p}, \vec{k}), \quad (11.3.9)$$

where $\Phi(\vec{p}, \vec{k})$ is given by 4 diagrams of Kohn-Luttinger [11.4] (see Fig. 11.2.)

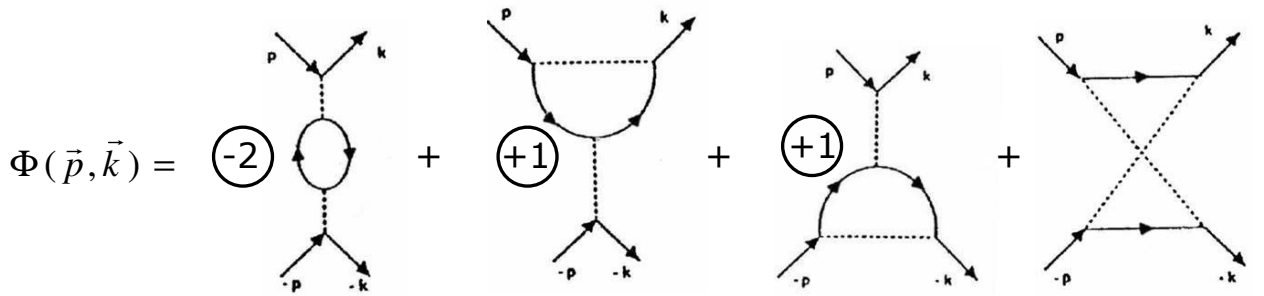


Fig. 11.2. Four diagrams of Kohn-Luttinger which give the contribution to the irreducible bare vertex for the Cooper channel.

First three diagrams cancel each other exactly for contact interaction and as a result in accordance with (11.3.3):

$$\Phi(\vec{p}, \vec{k}) = \Pi(\vec{p} + \vec{k}) \quad (11.3.10)$$

is given by fourth diagram on Fig. 11.2. Algebraically $\Pi(\vec{p} + \vec{k})$ is a static polarization operator (11.3.4) in a “crossed” channel (for $\tilde{q} = |\vec{p} + \vec{k}|$ instead of $q = |\vec{p} - \vec{k}|$). For incoming and outgoing momenta \vec{p} and \vec{k} lying on the Fermi-surface $|\vec{p}| = |\vec{k}| = p_F$ the “crossed” momentum:

$$\tilde{q}^2 = 2p_F^2(1 + \cos\theta), \quad (11.3.11)$$

where an angle $\theta = \angle \vec{p}\vec{k}$.

The polarization operator $\Pi(\tilde{q})$ is given by static Lindhard function [11.23]:

$$\Pi(\tilde{q}) = \frac{N_{3D}(0)}{2} \left[1 + \frac{4p_F^2 - \tilde{q}^2}{4p_F\tilde{q}} \ln \frac{2p_F + \tilde{q}}{|2p_F - \tilde{q}|} \right] \quad (11.3.12)$$

Integration of $\Pi(\tilde{q})$ with first Legendre polynomial $P_1(\cos\theta) = \cos\theta$ yields the desired result for p-wave harmonic [11.17, 11.18]:

$$\Pi_1 = \int_{-1}^1 P_1(\cos\theta) \frac{d\cos\theta}{2} \Pi(\tilde{q}(\cos\theta)) = \frac{N_{3D}(0)}{5} (1 - 2\ln 2) < 0. \quad (11.3.13)$$

The p-wave critical temperature reads:

$$T_{c1} \sim \frac{2e^C}{\pi} e^{\frac{13}{\lambda^2}}, \quad (11.3.14)$$

where $\lambda = 2a p_F/\pi$ in 3D is effective gas-parameter of Galitskii [11.2].

11.3.3. Model-independent considerations of Prof. P.Nozieres.

The model-independent proof of the possibility of the p-wave pairing in Fermi-systems with repulsion belongs to Prof. P.Nozieres [11.24]. His way of reasoning is the following: usually for static effective interaction in fermionic substance we have [11.23, 11.25]:

$$U_{\text{eff}}(q) = \frac{U_0(q)}{\varepsilon(q)}, \quad (11.3.15)$$

where $\varepsilon(q) = 1 + U_0(q)\Pi(q)$ is static dielectric function and $\Pi(q)$ is polarization operator given by (11.3.4). It is known from solid-state physics [11.21, 11.23] that $\Pi(q)$ is decreasing function of q which behaves as follows (see Fig. 11.3.).

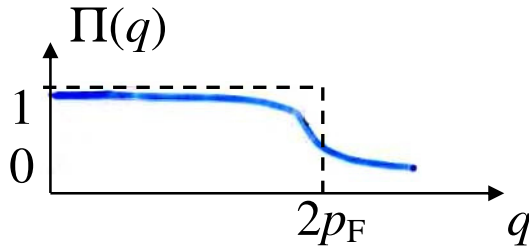


Fig. 11.3. Behavior of static polarization operator $\Pi(q)$ as a function of q with the decrease for $0 < q \leq 2p_F$.

That is why effective interaction U_{eff} in (11.3.15) decreases in the interval $0 \leq q \leq 2p_F$ which is important for superconductivity (see Fig. 11.4.).

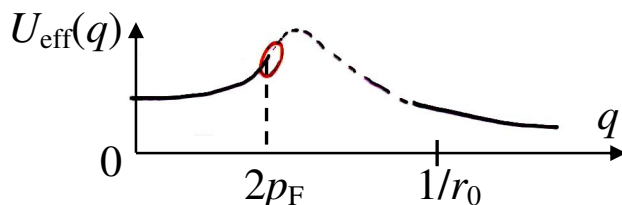


Fig. 11.4. Behavior of effective interaction U_{eff} as a function of q .

Note that $U_{\text{eff}}(q)$ should strongly decrease for $q > 1/r_0$, where r_0 is the range of the potential. But in the Fermi-gas $1/r_0 \gg 2p_F$ according to (11.3.1) and hence an interval $[0, 2p_F]$ where $U_{\text{eff}}(q)$ increases is an intermediate asymptotics (see Fig. 11.4).

Finally for first Legendre polynomial (which corresponds to p-wave pairing) we have:

$$q^2 = 2p_F^2(1 - \cos\theta), \quad (11.3.16)$$

and accordingly

$$P_1(\cos\theta) = \cos\theta = 1 - \frac{q^2}{2p_F^2} \quad (11.3.17)$$

Moreover $\cos\theta = 1$ for $q = 0$ and -1 for $q = 2p_F$. Thus $U_{\text{eff}}(\cos\theta)$ and $\cos\theta$ behave as follows (see Fig. 11.5.) as functions of $\cos\theta$.

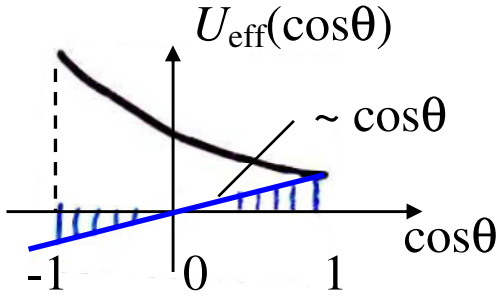


Fig. 11.5. Behavior of $U_{\text{eff}}(\cos\theta)$ and $\cos\theta$ as a function of $\cos\theta$ on the relevant interval $[-1, 1]$.

As a result the p-wave harmonic of U_{eff} :

$$U_{\text{eff}}^{l=0} = \int_{-1}^1 U_{\text{eff}}(\cos\theta) \cos\theta \frac{d\cos\theta}{2} < 0 \quad (11.3.18)$$

if $U_{\text{eff}}(\cos\theta)$ for $\cos\theta \in [-1, 0]$ is larger then $U_{\text{eff}}(\cos\theta)$ for $\cos\theta \in [0, 1]$ as in Fig. 11.5. Hence for all effective potential increasing for q changing from 0 to $2p_F$ we have p-wave SC in the isotropic case and the Kohn's anomaly does not play a decisive role here (in contrast with the case of SC pairing with large orbital momenta $l \gg 1$). Note that in 3D Fermi-gas model $U_{\text{eff}}(\cos\theta)$ is given by (11.3.3) and decreases on the interval $[-1, 1]$ due to crossing $q \rightarrow \tilde{q}$ (see (11.3.9)).

11.3.4. Two-dimensional case.

In 2D Fermi-gas with repulsion dimensionless effective interaction in momentum space reads:

$$N_{2D}(0)U_{\text{eff}}(\tilde{q}) = f_0 + f_0^2 \Pi(\tilde{q}) \frac{4\pi}{m}, \quad (11.3.19)$$

where $N_{2D}(0) = \frac{m}{2\pi}$ is 2D density of states,

$$f_0 = \frac{1}{2\ln(1/p_F r_0)} \quad (11.3.20)$$

is 2D gas-parameter of Bloom [11.3]. Correspondingly in real space effective interaction

$$N_{2D}(0)U_{\text{eff}}(r) \sim f_0^2 \frac{\cos(2p_F r)}{(2p_F r)^2} \quad (11.3.21)$$

contains much more stronger 2D Friedel oscillations [11.22].

However the 2D Kohn's anomaly [11.21] in polarization operator $\Pi(q)$ has one-sided character

$$N_{2D}(0)U_{\text{eff}}(\tilde{q}) \sim f_0^2 \text{Re} \sqrt{\tilde{q} - 2p_F} = 0 \quad (11.3.22)$$

for the important interval for SC $0 \leq \tilde{q} \leq 2p_F$. Hence strong 2D Kohn's anomaly is ineffective for SC in second order of perturbation theory with respect to gas-parameter f_0 (11.3.20). As it was shown by Chubukov [11.26] SC appears only in the third order of perturbation theory where the Kohn's anomaly changes its character first diagram on (Fig. 11.6) and reads:

$$N_{2D}(0)U_{\text{eff}}(\tilde{q}) \sim f_0^3 \text{Re} \sqrt{2p_F - \tilde{q}} \neq 0 \quad (11.3.23)$$

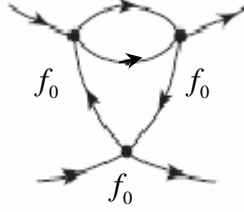


Fig. 11.6. Third order diagrams which contribute to effective interaction and SC in 2D Fermi-gas according to [11.26, 11.28]. First diagram on this figure was originally evaluated in [11.26] by Chubukov.

Accordingly critical temperature of the p-wave pairing reads in [11.26]:

$$T_{c1} \sim \varepsilon_F \exp \left\{ -\frac{1}{4.1 f_0^3} \right\} \quad (11.3.24)$$

Note that the first third order diagram on Fig. 11.6 considered in [11.26] is still irreducible with respect to Cooper channel.

Later on the authors of [11.27] and [11.28] considered all irreducible skeleton diagrams of the third order in f_0 on Fig. 11.6 on equal grounds and obtained $-6.1 f_0^3$ (instead of $-4.1 f_0^3$) in the exponent of (11.3.24) for p-wave pairing critical temperature in 2D Fermi-gas.

11.4. SC in 3D and 2D Hubbard model with repulsion at low electron density.

One of the basic models to describe unconventional normal and superconductive states of strongly-correlated electron systems is a famous Hubbard model originally introduced by Hubbard [11.29] for the explanation of metal-insulator transition in half-filled narrow band metals. In real space the Hamiltonian of the Hubbard model reads:

$$\hat{H}' = \hat{H} - \mu \hat{N} = -t \sum_{\langle i j \rangle \sigma} c_{i\sigma}^\dagger c_{j\sigma} + U \sum_i n_{i\uparrow} n_{i\downarrow} - \mu \sum_i n_{i\sigma}, \quad (11.4.1)$$

where $n_{i\sigma} = c_{i\sigma}^\dagger c_{i\sigma}$ is electron density with spin-projection $\sigma = |\uparrow \downarrow\rangle$ on site i , t – is hopping integral, U is on site Hubbard repulsion between two electrons with opposite spin-projections, μ is chemical potential.

11.4.1. 3D Hubbard model at low density.

After Fourier transformation the Hamiltonian (11.4.1) reads:

$$\hat{H}' = \sum_{\vec{p}\sigma} [\varepsilon(\vec{p}) - \mu] c_{\vec{p}\sigma}^\dagger c_{\vec{p}\sigma} + U \sum_{\vec{p}\vec{p}'\vec{q}} c_{\vec{p}\uparrow}^\dagger c_{\vec{p}'+\vec{q}\downarrow}^\dagger c_{\vec{p}+\vec{q}\downarrow} c_{\vec{p}'\uparrow}, \quad (11.4.2)$$

where $\varepsilon(\vec{p}) = -2t(\cos p_x d + \cos p_y d + \cos p_z d)$ is uncorrelated electron spectrum in 3D simple cubic lattice, d is intersite distance [11.29, 11.30, 11.31]. For small electron densities $nd^3 < 1$ (where $n = p_F^3/3\pi^2$ – electron density in 3D) the spectrum reads:

$$\varepsilon(p) \approx -\frac{W}{2} + tp^2 d^2, \quad (11.4.3)$$

where $W = 12t$ is a bandwidth in 3D for the simple cubic lattice. If we introduce the uncorrelated band mass according to [11.32]:

$$m = \frac{1}{2td^2}, \quad (11.4.4)$$

then for the spectrum we have:

$$\varepsilon(p) = -\frac{W}{2} + \frac{p^2}{2m}. \quad (11.4.5)$$

Correspondingly for the chemical potential at low densities:

$$\mu = -\frac{W}{2} + \varepsilon_F. \quad (11.4.6)$$

Thus according to [11.30, 11.31, 11.32] the 3D Hubbard model at low electron densities becomes equivalent to 3D Fermi-gas with δ -functional (hard-core) repulsive interaction between particles. The s-wave scattering length a in the renormalization scheme of Kanamori for Hubbard interaction [11.33, 11.34] reads:

$$\frac{4\pi a}{m} = T = \frac{Ud^3}{1 - Ud^3 K_{vac}(0,0)}, \quad (11.4.7)$$

where T – is a T-matrix, $K_{vac}(0,0) = -\int \frac{d^3 \vec{p}}{(2\pi)^3} \frac{m}{p^2}$ – is a Coper loop for two particles in vacuum

for total frequency $\Omega = 0$ and total momentum of two particles $\vec{P} = \vec{p}_1 + \vec{p}_2 = 0$.

Diagrammatically K_{vac} is a product of two vacuum Green-functions, while Lipman-Shwinger equation [11.35] for the T-matrix is illustrated on Fig. 11.11.

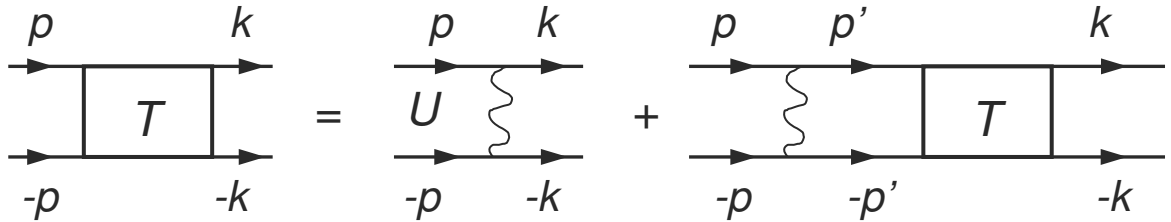


Fig. 11.11. Lipman-Shwinger equation (Bethe-Salpeter equation in vacuum) for the T-matrix [11.19, 11.35] in Kanamori renormalization scheme for Hubbard interaction.

In the strong-coupling limit $U \gg W$ of the Hubbard model and at low density we have according to [11.33] (see also [11.36]):

$$a \sim d \quad (11.4.8)$$

and thus effective gas-parameter for the Hubbard model reads:

$$\lambda = \frac{2ap_F}{\pi} = \frac{2dp_F}{\pi} \quad (11.4.9)$$

Correspondingly, in analogy with 3D Fermi-gas model, the Hubbard model at low electron density is unstable towards triplet p-wave pairing below the critical temperature [11.30-11.32]

$$T_{cl} \sim \varepsilon_F \exp\left\{-\frac{13}{\lambda^2}\right\}, \quad (11.4.10)$$

where λ is given by (11.4.9). Note that in the absence of the lattice for strong short-range interaction $a \sim r_0$, where r_0 is the range of the potential.

11.4.2. 2D Hubbard interaction.

The uncorrelated electron spectrum for 2D square lattice reads:

$$\varepsilon(p) = -2t(\cos p_x d + \cos p_y d) \quad (11.4.11)$$

Correspondingly, for low electron density $nd^2 \ll 1$ (where $n = p_F^2/2\pi$ is 2D electron density) the spectrum reads again (see (11.4.4) and (11.4.5)):

$$\varepsilon(p) \approx -\frac{W}{2} + \frac{p^2}{2m}, \quad (11.4.12)$$

the band mass is still $m = \frac{1}{2td^2}$, but now $W = -8t$ - a bandwidth for 2D square lattice.

Correspondingly, the chemical potential $\mu \approx -\frac{W}{2} + \varepsilon_F$ is given again by (11.4.6).

It is convenient to introduce dimensionless 2D density of electrons:

$$n_{el} = \frac{2\varepsilon_F}{W} \quad (11.4.13)$$

which measures the filling of the band in terms of the half-filled band ($n_{el} = 1$ for $\varepsilon_F = \frac{W}{2}$ in the half-filled case actual for high- T_C superconductors).

The gas-parameter of 2D Hubbard model at the strong-coupling limit $U \gg W$ and low density was derived in [11.37] and reads:

$$f_0 = \frac{1}{\ln(4W/\varepsilon_F)} = \frac{1}{\ln(8/n_{el})} \quad (11.4.14)$$

Correspondingly, in similarity with 2D Fermi-gas model the normal state of 2D Hubbard model at low density is unstable towards triplet p-wave pairing below the critical temperature [11.26-11.28, 11.31, 11.32].

$$T_{C1} \sim \varepsilon_F \exp\left\{-\frac{1}{6.1f_0^3}\right\} \quad (11.4.15)$$

with gas-parameter f_0 given by (11.4.14).

11.4.3. Qualitative phase-diagram at low density in 2D.

It is interesting to construct qualitative phase-diagram for different SC-instabilities in the 2D Hubbard model at low electron densities. This project was realized in [11.32]. To do that it is important to note (see [11.32]) that p-wave pairing with critical temperature given by (11.4.15) is the most energetically beneficial (corresponds to the highest T_C) for $U \gg t$ and dimensionless electron density $0 < n_{el} = \frac{2\varepsilon_F}{W} \leq 2/3$. In the same time in the weak-coupling case $U \leq 0.3 t$ and $0 < n_{el} \leq 2/3$ the highest T_C corresponds to d_{xy} -pairing according to [11.32] and [11.38]. For d_{xy} -pairing it is important to take into account the quadratic corrections to parabolic spectrum:

$$\varepsilon(p) - \mu = -2t(\cos p_x d + \cos p_y d) - \mu = \frac{p^2 - p_F^2}{2m} - \frac{(p_x^4 + p_y^4)d^2}{24m} \quad (11.4.16)$$

We should also remember that the superconductive gap for d_{xy} -pairing is given by [11.38]:

$$\Delta_{d_{xy}} \sim \Delta_0^d \sin(p_x d) \sin(p_y d) \sim \Delta_0^d p_x p_y d^2 \sim \Delta_0^d \sin 2\varphi \quad (11.4.17)$$

for low electron density, where φ is the angle between momentum \vec{p} and x -axis of the square lattice. In the same time more traditional $d_{x^2-y^2}$ -pairing actual for optimally doped high- T_C materials [11.39] correspond to the gap [11.38, 11.40]:

$$\Delta_{d_{x^2-y^2}} \sim \Delta_0^d (\cos p_x d - \cos p_y d) \sim \Delta_0^d (p_x^2 - p_y^2) d^2 \sim \Delta_0^d \cos 2\varphi \quad (11.4.18)$$

The critical temperature of d_{xy} -pairing is given by (see [11.38]):

$$T_C^{d_{xy}} \sim \varepsilon_F \exp \left\{ -\frac{20}{f_0^2 n_{el}^2} \right\} \quad (11.4.19)$$

In contrast to p-wave pairing it is described by the second-order (in the gas-parameter f_0) contribution to the effective interaction U_{eff} . This result [11.38] for d_{xy} -pairing was confirmed later on by Zanchi and Schulz [11.41] in the framework of renormalization group (RG) approach. We can also mention in this respect the papers of Hlubina et al. in which the authors get d_{xy} -pairing in weak-coupling case for $n_{el} \leq 0.62$ [11.64]. Finally for larger electron densities $n_{el} \geq 2/3$ both in weak-coupling ($U \ll W$) and strong-coupling case $d_{x^2-y^2}$ -pairing (which is more conventional for optimally doped high- T_C materials) is realized [11.42-11.47]. As a result the qualitative phase-diagram of the repulsive- U Hubbard model at low and moderate electron densities in 2D case looks like as follows (see Fig. 11.8).

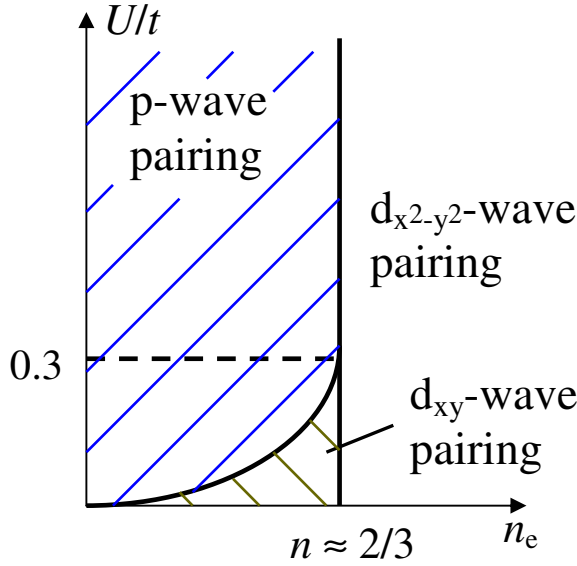


Fig. 11.8. Qualitative phase-diagram for SC-pairing in the 2D Hubbard model at low and moderate electron densities.

11.4.4. SC in 2D Hubbard model at larger electron densities $n_{el} \leq 1$.

At larger densities $n_{el} \leq 1$ close to half-filling $\left(\varepsilon_F \approx \frac{W}{2} \right)$ the spectrum of electrons becomes almost hyperbolic [11.44,11.45]:

$$\varepsilon(p) = \pm \frac{(p_x^2 - p_y^2)}{2m} \quad (11.4.20)$$

close to the corner points where the Fermi-surface almost touches the Brillouin zone $(0, \pi)$; $(0, -\pi)$ and $(\pi, 0)$; $(-\pi, 0)$ (see Fig. 11.9).

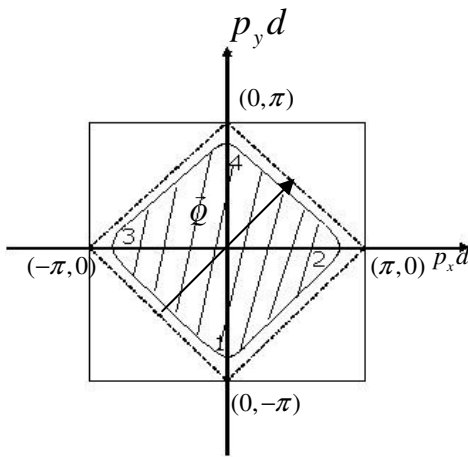


Fig. 11.9. Almost half-filling situation ($n_{el} \rightarrow 1$) for the 2D Hubbard model on the square lattice. At the corner points $(0, \pi)$; $(0, -\pi)$ and $(\pi, 0)$; $(-\pi, 0)$ the Fermi-surface

almost touches the Brillouin zone. We also show the nesting-vector $\vec{Q} = \left(\frac{\pi}{d}, \frac{\pi}{d}\right)$ on the figure.

There are here the extended almost flat parts of the Fermi-surface which satisfy the perfect nesting criteria for exactly half-filled case ($n_{el} = 1$).

$$\varepsilon(\vec{P} + \vec{Q}) = -\varepsilon(\vec{P}), \quad (11.4.21)$$

where $\vec{Q} = (\pi/d, \pi/d)$ is a nesting-vector for the 2D square lattice.

As a result the Kohn's anomaly becomes logarithmically strong here as in 1D-case (see [11.21,11.45]). Additional increase for T_C is due to Van-Howe singularity in the density of states $N_{2D}(0)$ which is also logarithmically strong [11.23,11.45]. As a result both polarization operator

$\Pi(q)$ in (11.3.4) and the Cooper loop (in substance) $K(0,0) = \int \frac{1-2n_F(\varepsilon_p)}{2(\varepsilon_p - \mu)} \frac{d^2 \vec{p}}{(2\pi)^2}$ contains \ln^2 -contribution. Thus in the weak-coupling case for the coupling constant

$$f_0 = \frac{U}{8\pi t} \ll 1 \quad (11.4.22)$$

and in the second order of perturbation theory (in f_0) for the effective interaction we have:

$$U_{\text{eff}} \sim f_0 + f_0^2 \ln^2 \frac{\mu}{t}, \quad (11.4.23)$$

where $\mu \ll t$ is chemical potential close to half-filling and we still assume that $\mu > T_C^d$. Note that in the expansion (11.4.23) an effective parameter of the perturbation theory is [11.44]:

$$f_0 \ln^2 \frac{\mu}{t}, \quad (11.4.24)$$

Correspondingly as it was shown by Kozlov [11.44] the equation for the $d_{x^2-y^2}$ -wave critical temperature T_C^d reads:

$$f_0^2 \ln^3 \frac{t}{\mu} \ln^2 \frac{\mu}{T_C^d} \sim 1 \quad (11.4.25)$$

or equivalently

$$T_C^d \sim \mu \exp \left\{ -\frac{1}{f_0^2 \ln^3 \frac{t}{\mu}} \right\}. \quad (11.4.26)$$

Thus we see that small coupling constant $f_0 \ll 1$ (11.4.22) is enhanced by large value of $\ln^3 \frac{t}{\mu} \gg 1$ in (11.4.26) – nice result of Kozlov. For the sake of completeness let us mention here the other important articles where $d_{x^2-y^2}$ -wave pairing with rather high T_C was obtained by a variety of computational approaches for 2D Hubbard model at optimal doping $n_{el} \sim (0.8 \div 0.9)$ [11.67-11.73, 11.78].

11.4.5. Parquette solution at weak-coupling and close to half-filling.

Very close to half-filling when $\mu \sim T_C$ we have so-called doubly-logarithmic parquette solution of Dzyaloshinslii, Yaroshenko [11.45] with the competition between SC and SDW-instability in particle-particle (SC) and particle-hole (SDW – spin density wave) channels. Here for $\mu \sim T_C$ from (11.4.26) we get:

$$f_0^2 \ln^4 \frac{t}{\mu} \sim f_0^2 \ln^4 \frac{t}{T_C^d} \sim 1 \quad (11.4.27)$$

Hence for the $d_{x^2-y^2}$ -wave critical temperature:

$$T_C^d \sim t \exp \left\{ -\frac{const}{\sqrt{f_0}} \right\} - \quad (11.4.28)$$

- an elegant result of [11.45]. We should mention here also the results of [11.74-11.78]. The maximal critical temperature in the 2D Hubbard model according to qualitative considerations of Kivelson et al. [11.48,11.48,11.65] corresponds to intermediate coupling case $U/W \sim 1$ and optimal concentrations $n_{el} \sim (0.8 \div 0.9)$. T_C here can reach the desired values of 10²K realistic for optimally doped cuprates [11.66].

The border between AFM (or SDW) phase and superconductive phase of the high- T_C superconductor (described by 2D Hubbard model) in weak-coupling case $U \ll W$ and very close to half-filling (for doping concentrations $x = (1 - n_{el}) \ll 1$) according to Kirelson [11.48] at the temperature $T \rightarrow 0$ is given by:

$$x_C = (1 - n_{el}) \sim \exp \left\{ -2\pi \sqrt{\frac{t}{U}} \right\} \quad (11.4.29)$$

and we have the same expression for $\frac{1}{\sqrt{f_0}} \sim \sqrt{\frac{t}{U}}$ in the exponent of (11.4.29) for x_C .

Another interesting observation belongs to Kopaev and Belyavsky [11.48] namely that the spectrum (11.4.11) on the square lattice at half-filling satisfies also “mirror nesting” property:

$$\mathcal{E}(P) = -\mathcal{E}(-P + Q) \quad (11.4.30)$$

This property is in favor of Cooper pairing with large total moment of a pair \vec{Q} in a clean case (no impurities).

11.5. SC transitions in the jelly model for Coulomb electron plasma.

Very recently in connection with the high- T_C physics Alexandrov and Kabanov [11.49] raised the very important question of the role of full Coulomb interaction (which is not reduced to onsite Hubbard repulsion but is extended over several coordinate spheres) for non-phonon mechanisms of superconductivity. They claimed that in the 3D jelly model for reasonable electron densities $r_s \leq 20$, where

$$r_s = \frac{1.92}{p_F a_B} \quad (11.5.1)$$

is correlative radius and $a_B = \frac{1}{me^2}$ ($\hbar = 1$) is Bohr radius for electron, the superconductive critical temperatures correspond to the pairing with large orbital momenta ($l \gg 1$) and are very low.

Indeed both the perturbative analysis of Chubukov and Kagan [11.50] (see also [11.31]) as well as numerical calculations of Alexandrov and Kabanov [11.49] provide small critical temperatures in 3D dense electron plasma.

11.5.1. Cascade of SC-transitions in the dense electron plasma.

To be more specific the authors of [11.50] predicted a cascade of SC-transitions with orbital moment of the Cooper pair l being dependent upon electron density r_s :

$$l > l_c = \frac{|\ln r_s|}{\sqrt{r_s}} \left(1 + \frac{7}{2} \frac{\ln |\ln r_s|}{|\ln r_s|} + \dots \right) \quad (11.5.2)$$

The critical temperature of the superconductive transition:

$$T_C \sim \varepsilon_F \exp \left\{ - \left(\frac{\pi}{4} \right)^2 \frac{1}{l^4} \right\} \quad (11.5.3)$$

corresponds for given density r_s to $l = l_c(r_s)$ from (11.5.2) and is very low. The authors of [11.79] get qualitatively the same result numerically with maximal but still very low T_C corresponding to f-wave pairing ($l = 3$) for $0 < r_s \leq 18$. We can honestly say that the 3D jelly model is not very promising for superconductivity with reasonable high- T_C in case of dense Coulomb plasma.

11.5.2. The dilute electron plasma.

The possibility of the p-wave SC with critical temperatures T_{C1} in the range $\sim (10^{-3} \div 10^{-2})$ K for 3D electron plasma of intermediate and small electron densities ($r_s \gg 1$) (which are relevant for simple and noble metals like Na, K, Ag, Au or for semimetals) was predicted in the papers [11.52-11.54]. Here $T_{C1} \sim \varepsilon_F \exp \{ -1/|\lambda_1| \}$, where $|\lambda_1| = 0.07$ in [11.52] and $|\lambda_1| = 0.06$ in [11.54].

The most realistic region of densities for p-wave pairing in 3D dilute plasma is possibly $20 \leq r_s \leq 35$ according to [11.52, 11.54]. In the same time some groups [11.55, 11.56] believe more in Khodel-Shaginyan [11.56] type of Fermi-surface reconstruction (and not SC-transition) at these densities or more close to Wigner crystallization instability. It is a very difficult question in particular in 2D where rigorously speaking we should sum up an infinite parquette class of diagrams for the effective interaction (irreducible bare vertex) U_{eff} in the Cooper channel.

11.6. SC in Shubin-Vonsovsky model at low density.

The situation for superconductivity with reasonable T_C becomes much more favorable on the lattice if we consider so-called Shubin-Vonsovsky model [11.55] with onsite Hubbard repulsion U and additional Coulomb repulsion V on the neighboring sites [11.56]. In real space the Hamiltonian of the Shubin-Vonsovsky model reads:

$$\hat{H}' = \hat{H} - \mu \hat{N} = -t \sum_{\langle i j \rangle \sigma} c_{i\sigma}^+ c_{j\sigma} + U \sum_i n_{i\uparrow} n_{i\downarrow} + \frac{V}{2} \sum_{\langle ij \rangle} n_i n_j - \mu \sum_{i\sigma} n_{i\sigma}, \quad (11.6.1)$$

where $n_i = \sum_{\sigma} n_{i\sigma}$ - total density on site i (for both \uparrow and \downarrow projection of electron spin. It is reasonable to assume (see [11.56]) that in (11.6.1) we have the following estimates for the parameters of the model:

$$U \sim \frac{e^2}{\varepsilon a_B}; \quad V \sim \frac{e^2}{\varepsilon d}; \quad W \sim \frac{1}{md^2}, \quad (11.6.2)$$

where W is a bandwidth, ε is the effective dielectric permittivity and $a_B \sim \frac{\varepsilon}{me^2}$ ($\hbar=1$) is Bohr radius in ionic media. Thus for $\varepsilon \sim 1$, $a_B \sim 0.5 \text{ \AA}$ and $d \sim (3 \div 4) \text{ \AA}$ [11.56] and in the limit $a_B/d \ll 1$ we come to the following hierarchy of parameters:

$$U \gg V \gg W. \quad (11.6.3)$$

The effective vacuum interaction in Shubin-Vonsovsky model in real space behaves as follows (see Fig. 11.10) in the strong-coupling case (11.6.3).

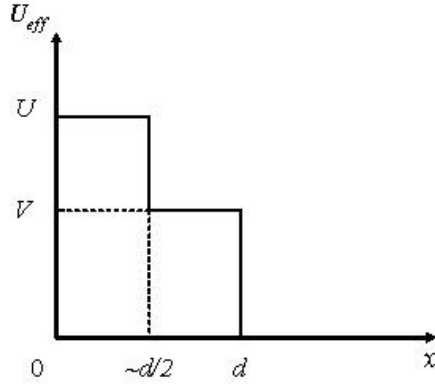


Fig. 11.10. Effective vacuum interaction in Shubin-Vonsovsky model in the strong-coupling case (11.6.3).

Note that Shubin-Vonsovsky model [11.55] is the most repulsive and the most unbeneficial model for SC. In the same time it is useful toy-model to study the effects of intersite Coulomb repulsion on SC and Mott-Hubbard metal-dielectric transition [11.29, 11.57] as well as the physics of the nanoscale phase separation [11.58, 11.59].

After Fourier transformation the Hamiltonian of the Shubin-Vonsovsky model reads:

$$\hat{H}' = \sum_{\vec{p}\sigma} [\varepsilon(p) - \mu] c_{p\sigma}^+ c_{p\sigma} + U \sum_{\vec{p}\vec{p}'\vec{q}} c_{\vec{p}\uparrow}^+ c_{\vec{p}'+\vec{q}\downarrow}^+ c_{\vec{p}+\vec{q}\downarrow} c_{\vec{p}'\uparrow} + \sum_{\substack{\vec{p}\vec{p}'\vec{q} \\ \sigma\sigma'}} V(\vec{p}, \vec{p}') c_{\vec{p}\sigma}^+ c_{\vec{p}'+\vec{q}\sigma'}^+ c_{\vec{p}+\vec{q}\sigma} c_{\vec{p}'\sigma'}, \quad (11.6.4)$$

where in 3D case:

$$V(\vec{p}, \vec{p}') = V(\cos(p_x - p_x')d + \cos(p_y - p_y')d + \cos(p_z - p_z')d) \quad (11.6.5)$$

At the low density $pd \ll 1$ the expansion up to quadratic terms gives effective vacuum interaction in 3D for s-wave and p-wave harmonics respectively:

$$U_{\text{eff vac}}^S = U + 6V + o(p^2 d^2), \quad (11.6.6)$$

and

$$U_{\text{eff vac}}^P = 2V\vec{p}\vec{p}'d^2 \quad (11.6.7)$$

The renormalization of effective vacuum interaction in the framework of Kanamori T-matrix approximation [11.33] yields for s-wave and p-wave scattering lengths [11.58] in the strong-coupling $U \gg V \gg W$ and low density $nd^3 < 1$ case:

$$a_s \sim d, \quad (11.6.8)$$

and

$$a_p \sim d, \quad (11.6.9)$$

where $T_s = \frac{4\pi a_s}{m}$ and $T_p = \frac{4\pi}{m} 2a_p(\vec{p}\vec{p}')d^2$ are T-matrices in s-wave and p-wave channels.

Thus the dimensionless s-wave gas-parameter $\lambda_s = \lambda = 2d p_F/\pi$ as in the repulsive- U Hubbard model (see (11.9.4)) while the dimensionless p-wave gas-parameter:

$$\lambda_p \sim (p_F d)^3 \quad (11.6.10)$$

in agreement with general quantum-mechanical consideration for slow particles ($p_F d < 1$) in vacuum (see [11.35]).

Thus in 3D a normal state of the Shubin-Vonsovsky model at strong-coupling and low densities is again unstable towards triplet p-wave pairing. The irreducible bare vertex in substance reads:

$$N_{2D}(0)U_{\text{eff}}^{l=1} = \lambda_s^2 \Pi_{l=1} + \lambda_p \quad (11.6.11)$$

Thus critical temperature in the main order of the s-wave gas-parameter is given by (11.4.10) again.

The presence of the additional Coulomb repulsion V on the neighboring sites in the model changes only the preexponential factor in (11.4.10). Thus situation in the 3D Shubin-Vonsovsky model and low electron density is much more favorable for SC with reasonable T_C even in the

most repulsive strong-coupling case (in contrast with the situation in 3D jelly model for dense electron plasma).

Analogously in strong-coupling and low density 2D case the s-wave dimensionless gas-parameter is again $f_s = f_0 = \frac{1}{\ln(4W/\epsilon_F)} = \frac{1}{\ln(8/n_{el})}$ (see (11.4.14)) as in the 2D Hubbard model, while the dimensionless p-wave gas-parameter:

$$f_p \sim p_F^2 d^2 \quad (11.6.13)$$

in 2D again in agreement with general quantum-mechanical considerations [11.35] for slow particles in vacuum. The irreducible bare vertex in substance reads in 2D:

$$U_{eff}^{l=1} N_{2D}(0) = -6.1 f_s^3 + 2 p_F^2 d^2 \quad (11.6.14)$$

Hence in the main order of 2D s-wave gas-parameter the p-wave critical temperature is given again by (11.4.15) in exact similarity with 2D Hubbard model. The presence of the additional Coulomb repulsion V again changes only the preexponential factor.

11.6.2. Localization and phase separation in Shubin-Vonsovsky model at larger densities.

At larger dimensionless densities $n_{el} \geq 0.5$ ($n_{el} = 0.5$ corresponds to quarter-filling of the band) there are, however, extended regions of phase-separation in Shubin-Vonsovsky model in the strong-coupling limit $U \gg V \gg W$.

To be more specific in the model [11.55] there are two types of localization: Mott-Hubbard localization with an appearance of AFM-state at half-filling ($n_{el} \rightarrow 1$) [11.29, 11.57] and Verwey localization with an appearance of checkerboard charge-ordered (CO) state at quarter-filling ($n_{el} \rightarrow 1/2$) [11.59].

Close to $n_{el} = 1/2$ and $n_{el} = 1$ we have extended regions of nano-scale phase-separation [11.56-11.58]. The qualitative phase-diagram of the Shubin-Vonsovsky model in the strong-coupling case is presented on Fig.11.11.

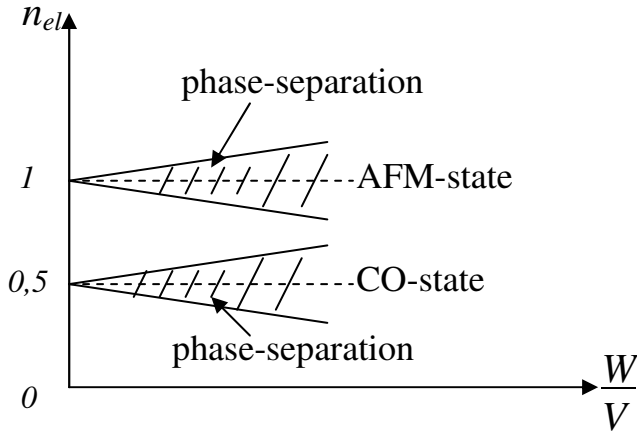


Fig.11.11. Qualitative phase-diagram of the Shubin-Vonsovsky model in the strong-coupling case. At $n_{el} = 1$ AFM-state appears in the model, while at $n_{el} = 1/2$ we have the checkerboard CO-state.

If we increase the density from $n_{el} \rightarrow 0$ to $n_{el} = 1/2 - x$, then at the critical concentrations:

$$x_c \sim \left(\frac{W}{V}\right)^{3/5} \quad \text{in 3D} \quad (11.6.16)$$

and

$$x_C \sim \left(\frac{W}{V}\right)^{1/2} \text{ in 2D} \quad (11.6.17)$$

the system undergoes the first-order phase-transition into a phase-separated state with nano-scale metallic clusters inside charge-ordered checkerboard insulating matrix (see Fig.11.12). At critical concentration $n_{el} = 1/2 - x_C$ the metallic clusters start to touch each other. As a result all the sample volume becomes metallic for $n_{el} < 1/2 - x_C$. The more detailed analysis of Verwey localization at $n_{el} = 1/2$ and nano-scale phase-separated state for $1/2 - x_C < n_{el} < 1/2$ will be a subject of Chapter 17.



Fig.11.12. Phase-separated state at the densities $1/2 - x_C < n_{el} < 1/2$ with nano-scale metallic clusters inside CO checkerboard insulating matrix. At critical concentration $n_{el} = 1/2 - x_C$ the metallic clusters start to touch each other and all the volume of the sample becomes metallic.

Thus we can not extend our calculations for T_C in homogeneous case to densities larger than $n_{el} = 1/2 - x_C$ in the strong-coupling limit of Shubin-Vonsovsky model. However it is interesting to construct SC phase-diagram of the model for $n_{el} < 0.5 - x_C$ and to find the regions of p-wave, d_{xy} and $d_{x^2-y^2}$ -pairing [11.56]. The work along these lines is in progress [11.61].

Another interesting problem is to consider the opposite weak-coupling Born case $W > U > V$ which can be realized for large Bohr radius $a_B > d$ or correspondingly for large dielectric permittivity $\epsilon \gg 1$ (note that real high- T_C materials are in the difficult intermediate coupling regime $\epsilon \geq 1$ and $a_B \sim d$). In the weak-coupling case Verwey localization [11.59] is absent for $n_{el} \rightarrow 1/2$ and we can construct superconductive phase-diagram of the Shubin-Vonsovsky model for p-wave, d_{xy} and $d_{x^2-y^2}$ -pairing for all densities including almost half-filled case [11.61].

The first numerical results in this respect were obtained in [11.65], where the authors found (besides p-wave, d_{xy} and $d_{x^2-y^2}$ -pairing) also the regions of extended s-wave pairing and g-wave pairing for $0 < n_{el} < 0.95$.

11.11 Reference to Chapter 11

- 11.1. J. Bardeen, L. N. Cooper, and J. R. Schrieffer, Phys. Rev., 108, 1175–1204 (1957); L. N. Cooper, Phys. Rev. 104, 1189–1190 (1956); J. R. Schrieffer, Theory of Superconductivity, Benjamin New York, 1964.
- 11.2. P. W. Anderson, Science 235, 1196–1198 (1987).
- 11.3. V.M. Galitskii, JETP 34, 151–162 (1958).
- 11.4. P. Bloom, Phys. Rev. B 12, 125–129 (1975).
- 11.5. W. Kohn, J. M. Luttinger, Phys. Rev. Lett., 15, 524–526 (1965).
- 11.6. C. M. Varma, P. B. Littlewood, S. Schmitt-Rink, E. Abrahams, A. E. Ruckenstein, Phys. Rev. Lett., 63, 1996–1999 (1989).
- 11.7. D. Vollhardt, P. Wölfle, The Superfluid Phases of Helium 3, Taylor and Francis, London, 1990.
- 11.8. G. E. Volovik, Exotic properties of superfluid 3He, World Scientific, Singapore, 1992.
- 11.9. C. A. Regal, C. Ticknor, J. L. Bohn, D. S. Jin, Phys. Rev. Lett., 90, 053201 (2003).
- 11.10. C. H. Schunck, M. W. Zwierlein, C. A. Stan, S. M. F. Raupach, W. Ketterle, A. Simoni, E. Tiesinga, C. J. Williams, P. S. Julienne, Phys. Rev. A 71, 045601 (2005).
- 11.11. H. R. Ott, H. Rudigier, T. M. Rice, K. Ueda, Z. Fisk, J. L. Smith, Phys. Rev. Lett., 52, 1915–1918 (1984); S. Kromer, R. Helfrich, M. Lang, F. Steglich, C. Langhammer, A. Bach, T. Michels, J. S. Kim, G. R. Stewart, Phys. Rev. Lett., 81, 4476–4479 (1998).

- 11.12. H.-Y. Kee, A. Raghavan, K. Maki, arXiv:0711.0929; Proc. of the First Euroconference on Anomalous Complex Superconductors, Crete (Greece) September 1998.
- 11.13. Y. Maeno, T. M. Rice, M. Sigrist, Phys. Today 54, 42 (2001); T. M. Rice, M. Sigrist, J. Phys.: Condens. Matter 7, L643 (1995).
- 11.14. J. G. Bednorz, K. A. Müller, Zeit. für Phys. B Cond. Matt., 64, 189-193 (1986); Physical properties of high temperature superconductors, edited by D. M. Ginsberg, World Scientific, Singapore, 1994; J. C. Phillips, Physics of High-Tc Superconductors, Academic Press, 1989; S. A. Wolf, V. Z. Kresin, Novel superconductivity, Plenum Press, 1987.
- 11.15. J. Nagamatsu, N. Nakagawa, T. Muranaka, Y. Zenitani, J. Akimitsu, Nature 410, 63-64 (2001)
- 11.16. Izumov High T_C superconductors on the basis of FeAs compounds, Publ. home R&C Dynamic, Moscow, 2009 (in Russian); Andrey V. Chubukov, Plenary talk in the Proc. of the Conference Stripes XI, Rome, Italy, July 2011; S. J. Bending et al., Plenary talk on 7th International Conference on Vortex Matter in Nanostructured Superconductors, Rhodes, Greece, September 2011.
- 11.17. L. R. Gor'kov, T. K. Melik-Barkhudarov, JETP 40, 1452-1460 (1961).
- 11.18. D. Fay, A. Layzer, Phys. Rev. Lett., 20, 187-190 (1968).
- 11.19. M. Yu. Kagan, A.V. Chubukov, JETP Lett., 47, 525-528 (1988).
- 11.20. E. M. Lifshitz, L. P. Pitaevskii, Statistical Physics, Part 2, Pergamon Press 1988.
- 11.21. A. A. Abrikosov, L. P. Gorkov, I. E. Dzialoshinskii, Methods of Quantum Field Theory in Statistical Physics, Prentice Hall, 1963.
- 11.22. W. Kohn, Phys. Rev. Lett., 2, 393-394 (1959).
- 11.23. J. Friedel, Adv. Phys. 3, 446 (1954).
- 11.24. J. Lindhard, Kgl. Danske Videnskab, Selskab, Mat.-Fys. Medd., 28, No. 8 (1954); N. W. Ashcroft, N. D. Mermin, Solid State Physics, Vol. 1, Holt, Rinehart and Winston, 1976.
- 11.25. P. Nozieres, private communication to the author.
- 11.26. M. Yu. Kagan, A.V. Ozharovskii, Basic mechanisms of superconductivity in strongly correlated electrom systems, Lecture course, Part II, Moscow, 1999.
- 11.27. A. V. Chubukov, Phys. Rev. B 48, 1097-1104 (1993).
- 11.28. M. A. Baranov, D. V. Efremov, M. S. Mar'enko, M. Yu. Kagan, JETP 90, 861 (2000).
- 11.29. D. V. Efremov, M. S. Mar'enko, M. A. Baranov, M. Yu. Kagan, Physica B 284-288, 216 (2000); M. S. Mar'enko, PhD Thesis, Kapitza Institute, Moscow, 2000.
- 11.30. J. Hubbard, Proc. R. Soc. Lond. A 276, 238-257 (1963); Proc. R. Soc. Lond. A 277, 237-259 (1964); Proc. R. Soc. Lond. A 281, 401-419 (1964); Proc. R. Soc. Lond. A 285, 542-560 (1965).
- 11.31. M. A. Baranov, M. Yu. Kagan, JETP 99, 1236-1240 (1991).
- 11.32. M. A. Baranov, A. V. Chubukov, M. Yu. Kagan, Int. J. Mod. Phys. B 6, 2471-2497 (1992).
- 11.33. M. Yu. Kagan, Superconductivity and superfluidity in Fermi-systems with repulsion, Habilitation thesis, Moscow, Kapitza Institute, 1994.
- 11.34. J. Kanamori, Prog. Theor. Phys., 30, 275-289 (1963).
- 11.35. M. Yu. Kagan, V.V. Val'kov, JETP 113, 156-171 (2011).
- 11.36. L. D. Landau, E. M. Lifshitz, Quantum Mechanics: Non-Relativistic Theory, Pergamon Press, 1977.
- 11.37. P. Fulde, Electron Correlations in Molecules and Solids, Springer, 1993.
- 11.38. H. Fukuyama, Y. Hasegawa, O. Narikiyo, J. Phys. Soc. Jpn., 60, 2013-2030 (1991).
- 11.39. M. A. Baranov, M. Yu. Kagan, Z. Phys. B-Cond. Matt., 86, 237-239 (1992).
- 11.40. D. A. Wollman, D. J. Van Harlingen, W. C. Lee, D. M. Ginsberg, A. J. Leggett, Phys. Rev. Lett., 71, 2134-2137 (1993).
- 11.41. M Yu Kagan and T M Rice, J. Phys.: Cond. Matt., 6, 3771-3780 (1994).
- 11.42. D. Zanchi, H. J. Schulz, Phys. Rev. B 54, 9509-9519 (1996).
- 11.43. K. Miyake, S. Schmitt-Rink, C. M. Varma, Phys. Rev. B 34, 6554-6556 (1986).

- 11.44. D. J. Scalapino, E. Loh, Jr., J. E. Hirsch, Phys. Rev. B 34, 8190–8192 (1986).
- 11.45. A. I. Kozlov, Supercond.: physics, chemistry, engineering 2, 64–68 (1989) (in Russian).
- 11.46. I. E. Dzyaloshinskii, V. M. Yakovenko, JETP 94, 344–355 (1988).
- 11.47. J. R. Schrieffer, X. G. Wen, S. C. Zhang, Phys. Rev. B 39, 11663–11679 (1989); A. Kampf, J. R. Schrieffer, Physica B 163, 267–270 (1990); A. Kampf, J. R. Schrieffer, Phys. Rev. B 41, 6399–6408 (1990).
- 11.48. S. Raghu, S. A. Kivelson, D. J. Scalapino, Phys. Rev. B 81, 224505 (2010).
- 11.49. S. A. Kivelson, Plenary talk on Strongly Correlated Electron Systems (SCES) Conference, Cambridge, UK, August - September 2011, S. Raghu, E. Berg, A.V. Chubukov and S.A. Kivelson, arxiv/cond-mat:1111.2982 (13 November 2011)
- 11.50. V.I. Belyavsky, V.V. Kapaev and Yu.V. Kopaev PRB, v.80, p. 214524 (2009); V.V. Belyavsky, Yu. V. Kopaev, PRB, v. 76, p. 214506 (2007)
- 11.51. A. S. Alexandrov, V. V. Kabanov, Phys. Rev. Lett., 106, 136403 (2011).
- 11.52. A. V. Chubukov, M. Yu. Kagan, J. Phys.: Conds. Matt., 1, 3135–3138 (1989).
- 11.53. J. Appel, H. Hetszenau, Phys. Rev. 188, 755–758 (1969).
- 11.54. S. Küchenhoff, P. Wölfle, Phys. Rev. B 38, 935–937 (1988).
- 11.55. K. Efetov, I. Aleiner, J. Phys.: Cond. Mat., 19, 255215 (2007).
- 11.56. V. A. Khodel, V. R. Shaginyan, JETP Lett., 51, 488–490 (1990).
- 11.57. S. V. Vonsovsky, Yu. A. Izumov, E. Z. Kurmaev, Superconductivity of Transition Metals, Their Alloys, and Compounds, Springer, 1982; S. Shubin, S. Vonsovsky, Proc. R. Soc. Lond. A 145, 159–180 (1934).
- 11.58. M. Yu. Kagan, D.V. Efremov, M. S. Mar'enko, V. V. Val'kov, JETP Lett., 93, 819–824 (2011).
- 11.59. N.F. Mott, E. A. Davis, Electronic Processes in Non-Crystalline Materials, Oxford University Press, 1979.
- 11.60. E. L. Nagaev, JETP Lett., 6, 484 (1967).
- 11.61. M. Yu. Kagan, K. I. Kugel, D.I. Khomskii, JETP 93, 415 (2001); M. Yu. Kagan, K. I. Kugel, Sov. Phys. Uspekhi 171, 577 (2001).
- 11.62. E. J. W. Verwey, Nature 144, 327–328 (1939); E. J. W. Verwey, P. W. Haayman, Physica 8, 979 (1941).
- 11.63. M. Yu. Kagan, V. V. Val'kov, M. M. Korovushkin, JETP 2012, to be published.
- 11.64. R. Hlubina, Phys. Rev. B, 59, p. 9600 (1999); J. Mraz and R. Hlubina, Phys. Rev. B, 67, p. 174518 (2003); ibid B, 69, p. 104501 (2004)
- 11.65. S. Raghu, E. Berg, A.V. Chubukov and S.A. Kivelson, Phys. Rev. B (2012) in press
- 11.66. A. Kanigel et al, Phys. Rev. Lett, 99, p. 157001 (2007)
- 11.67. B. Kyung et al., Phys. Rev. B, 68, p. 174502 (2003)
- 11.68. S.R. White, Phys. Rev. Lett., 69, p. 2863 (1992)
- 11.69. P. Monthoux and D.J. Scalapino, Phys. Rev. Lett, 72, p. 1874 (1994)
- 11.70. D. Manske et al., Phys. Rev. B, 67, p. 134520 (2003)
- 11.71. T. Maier et al., Phys. Rev. Lett., 95, p. 237001(2005)
- 11.72. K. Haule and G. Kotliar, Phys. Rev. B, 76, p. 104509 (2007)
- 11.73. S. Pathak, V.B. Shenoy, M. Randeria and N. Trivedi, Phys. Rev. Lett, 102, p. 027002 (2009)
- 11.74. K. Le. Hur and T.M. Rice, Annals of Physics, 325, p. 1452 (2009)
- 11.75. D. Podolsky, H.-Y. Kee, Y.B. Kim, Europhysics Letters, 88, p. 17004 (2009)
- 11.76. A.T. Zheleznyak, V.M. Yakovenko and I.E. Dzyaloshinskii, Phys. Rev. B, 55, p. 3200 (1997)
- 11.77. H.J. Shulz, Europhys. Lett., 4, p. 609 (1987)
- 11.78. P.A. Lee, N. Nagaosa and X.-G. Wen, Rev. Mod. Phys, 78, p. 17 (2006)

Chapter 12. Strong T_C enhancement in spin-polarized Fermi-gas and in two-band superconductors.

Content

- 12.1. T_C enhancement in spin-polarized neutral Fermi-gas.
 - 12.1.1. 3D spin-polarized Fermi-gas.
 - 12.1.2. 2D spin-polarized Fermi-gas.
 - 12.1.3. Spin-polarized superfluid ^3He .
- 12.2. T_C enhancement in quasi-2D charged SC in parallel magnetic field.
- 12.3. Strong T_C enhancement in the two-band model.
 - 12.3.1. The two-band Hubbard model with one narrow band.
 - 12.3.2. The Kanamori T-matrix approximation.
 - 12.3.3. Evaluation of the self-energies of heavy and light bands.
 - 12.3.4. Electron-polaron effect
 - 12.3.5. Other mechanisms of heavy mass enhancement. The tendency towards phase-separation.
 - 12.3.6. Anomalous (p-wave) SC in the two-band model. Enhanced Kohn-Luttinger effect.

In previous chapter (Chapter 11) we discuss the possible unconventional SC of p-wave and d-wave character in strongly correlated fermion systems with repulsive interaction between particles. The basic mechanism of SC which we discussed at low electron densities was Kohn-Luttinger mechanism [11.4] and its extension on triplet p-wave pairing by Fay, Laser [11.17] and Kagan, Chubukov [11.18]. However the critical temperatures of 3D and 2D p-wave pairing given by (11.4.10) and (11.4.14) are usually rather low, especially in 3D.

The legitimate question then appears whether it is possible to increase T_C already at low density and to get experimentally feasible critical temperatures?

The answer to this question is positive and is connected with 2 possibilities:

- 1) to apply external magnetic field (or strong spin-polarization) to triplet p-wave SC [12.1, 12.2];
- 2) to consider the two-band situation especially for multiband SC with one narrow band [12.3, 12.4].

In both cases the most important idea – is to separate the channels for the formation of Cooper pair and for the preparation of the effective interaction [12.1, 12.3].

12.1. T_C enhancement in spin-polarized neutral Fermi-gas.

In magnetic field (or in the presence of the strong spin-polarization) the Cooper pair according to [12.1] is formed by two fermions with spins “up”, while an effective interaction is prepared by two fermions with spins “down” (see Fig.12.1).

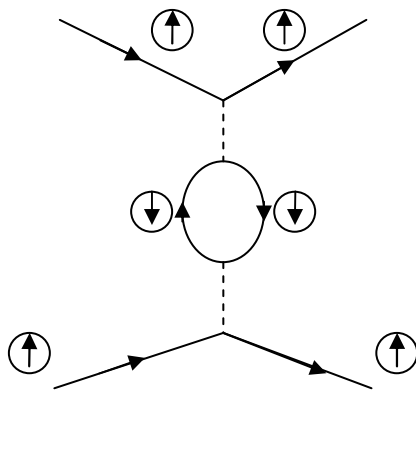
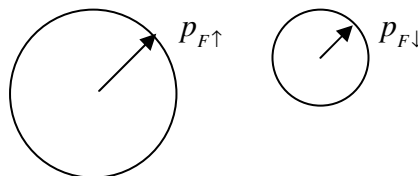


Fig.12.1. An idea of the separation of the channels for Cooper pairing and effective interaction in triplet neutral SC. An effective interaction is proportional to polarization operator $\Pi_{\downarrow\downarrow}(q)$ for “down” (with $p_{F\downarrow}$) spins in the second order of perturbation theory. The Cooper pair is formed by two spins “up” (with $p_{F\uparrow}$)



12.1.1. 3D spin-polarized Fermi-gas.

As a result the Kohn's anomaly is strongly increased. In the absence of magnetic field (for $H = 0$) the Kohn's anomaly in 3D reads: $(q - 2p_F) \ln|q - 2p_F|$ (see (11.3.5)) where $q^2 = 2p_F^2(1 - \cos\theta)$, (see (11.3.11)). Physically Kohn's anomaly is important for $q \rightarrow 2p_F$ (diameter of Fermi-sphere) or for angles $\theta \rightarrow \pi$ - backward scattering between incoming and outgoing momenta \vec{p} and \vec{k} for the Cooper channel ($q = |\vec{p} - \vec{k}|$; $|\vec{p}| = |\vec{k}| = p_F$). In terms of the angle θ between \vec{p} and \vec{k} ($\theta = \angle \vec{p}\vec{k}$) the Kohn's anomaly for $H = 0$ reads:

$$\Pi_{\text{sing}}(q) \sim (q - 2p_F) \ln|q - 2p_F| \sim (\pi - \theta)^2 \ln(\pi - \theta) \quad (12.1.1)$$

and only second derivative of $\Pi_{\text{sing}}(\theta)$ with respect to $(\pi - \theta)$ diverges. In the same time for $H \neq 0$ the Fermi-momenta for the particles with spins "up" and "down" are different ($p_{F\uparrow} \neq p_{F\downarrow}$) and thus:

$$\Pi_{\text{sing}}(\theta) \sim (q_{\uparrow} - 2p_{F\downarrow}) \ln|q_{\uparrow} - 2p_{F\downarrow}| \sim (\theta - \theta_C) \ln(\theta - \theta_C), \quad (12.1.2)$$

where θ_C differs from π proportionally to $(p_{F\uparrow} / p_{F\downarrow} - 1)$. Correspondingly already first derivative of $\Pi_{\text{sing}}(\theta)$ with respect to $(\theta - \theta_C)$ diverges. Unfortunately for $H \neq 0$ there is a competing process namely the decrease of the density of states of the fermions with "down" spins in $\Pi_{\downarrow\downarrow}(\theta)$ on Fig.12.1:

$$N_{\downarrow}^{3D}(0) = \frac{mp_{F\downarrow}}{2\pi^2} \quad (12.1.3)$$

As a result of this competition the critical temperature $T_C^{\uparrow\uparrow}$ (for Cooper pair formed by two "up" spins) has strongly non-monotonous (reentrant) behavior with large maximum (see Fig.12.2).

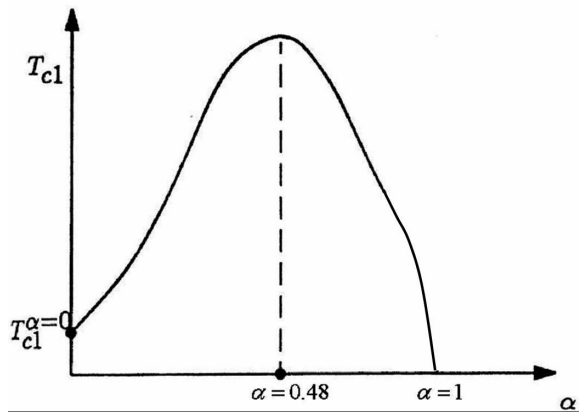


Fig.12.2. Dependence of the p-wave critical temperature $T_C^{\uparrow\uparrow}$ (for pairing of two "up" spins) from the degree of spin-polarization in 3D polarized Fermi-gas with repulsion.

In terms of the polarization degree:

$$\alpha = \frac{n_{\uparrow} - n_{\downarrow}}{n_{\uparrow} + n_{\downarrow}}, \quad (12.1.4)$$

where $n_{\uparrow} = p_{F\uparrow}^3 / 6\pi^2$ and $n_{\downarrow} = p_{F\downarrow}^3 / 6\pi^2$ are the densities of "up" and "down" fermions in 3D. the critical temperature has a pronounced maximum for $\alpha = 0.48$ (48% of the polarization). Correspondingly $\delta = p_{F\uparrow} / p_{F\downarrow} = 1.43$ at maximum [11.31, 12.1], where in 3D:

$$\alpha = \frac{\delta^3 - 1}{\delta^3 + 1} \quad (12.1.5)$$

Note that polarization operator $\Pi_{\downarrow\downarrow}(q)$ in Fig.12.1 reads in 3D:

$$\Pi_{\downarrow\downarrow}(q_{\uparrow}) = \frac{N_{\downarrow}^{3D}(0)}{2} \left[1 + \frac{4p_F^2 - q_{\downarrow}^2}{4p_{F\downarrow}q_{\uparrow}} \ln \frac{2p_{F\downarrow} + q_{\uparrow}}{|2p_{F\downarrow} - q_{\downarrow}|} \right] \quad (12.1.6)$$

Correspondingly in terms of $\delta = p_{F\uparrow}/p_{F\downarrow}$ from (12.1.5) and angle θ the transferred momentum squared $q_{\uparrow}^2 = 2p_{F\uparrow}^2(1 - \cos\theta)$ the polarization operator is given by:

$$\Pi_{\downarrow\downarrow}(\theta) = \frac{N_{\downarrow}^{3D}(0)}{2} \left[1 + \frac{1 - \delta^2 \sin^2 \frac{\theta}{2}}{2\delta \sin \frac{\theta}{2}} \ln \frac{1 + \delta \sin \frac{\theta}{2}}{|1 - \delta \sin \frac{\theta}{2}|} \right] \quad (12.1.7)$$

The evaluation of p-wave harmonics $\Pi_{\downarrow\downarrow}^{l=1}$ is again elementary and can be done analytically as in unpolarized case (for $\delta = 1$) (see [12.1]). For us it is important to represent

$$T_{C1}^{\uparrow\uparrow} = T_{C1}(\alpha = 0) e^{\frac{f(\alpha)}{\lambda^2}}, \quad (12.1.8)$$

(where $\lambda = 2a p_F/\pi$ is 3D gas-parameter) and show that for small $\alpha \ll 1$

$$f(\alpha) = \frac{5}{9} \alpha \frac{(7 - 4 \ln 2)}{(2 \ln 2 - 1)^2} > 0 \quad (12.1.9)$$

positive and linear in α . Note that for not very strong external magnetic field $\mu_B H < \varepsilon_{F0}$ ($\varepsilon_{F0} = p_{F0}^2/2m$ – Fermi-energy for $H = 0$) we have the linear relation between α and H :

$$\alpha \approx \frac{3}{2} \frac{\mu_B H}{\varepsilon_{F0}} \ll 1 \quad (12.1.10)$$

in 3D case. Thus $T_{C1}^{\uparrow\uparrow}$ increases for $\alpha \ll 1$. In the opposite case of practically 100% polarization ($\alpha \rightarrow 1$ or $1 - \alpha \rightarrow 0$) we have:

$$f(\alpha) = -\frac{9}{2^{2/3}} \frac{1}{(1 - \alpha)} \rightarrow -\infty \quad (12.1.11)$$

Hence $T_{C1}^{\uparrow\uparrow} \rightarrow 0$ for $\alpha \rightarrow 1$. The asymptotic behavior of $f(\alpha)$ for $\alpha \ll 1$ and $(1 - \alpha) \ll 1$ justifies the appearance of the maximum of $T_{C1}^{\uparrow\uparrow}$ in between. In maximum:

$$\max T_{C1}^{\uparrow\uparrow} = T_{C1}^{\uparrow\uparrow}(\alpha = 0.48) \sim \varepsilon_F e^{\frac{7}{\lambda^2}}, \quad (12.1.12)$$

and we see that in the second order of perturbation theory the expression in the main exponent for T_C increases practically in 2 times (from $\lambda^2/13$ to $\lambda^2/7$) giving a large T_C -enhancement in 3D spin-polarized Fermi-gas. Note that the behavior of the critical temperature at $\alpha \rightarrow 1$ is not accidental in this approximation, namely $T_{C1}^{\uparrow\uparrow}(\alpha = 1) = 0$ because of the absence of “down” spins in 100% polarized gas. $T_{C1}^{\uparrow\uparrow}(\alpha = 1)$ is non-zero only in the third order of the gas-parameter $\lambda = 2a p_F/\pi$ which is in accordance with Pauli principle for slow particles in vacuum [11.35] (p-wave harmonic of the scattering amplitude $f_l \sim (a p_F)^3$).

12.1.2. 2D spin-polarized Fermi-gas.

This effect is even more pronounced in 2D spin-polarized Fermi-gas. Here, as we discussed in Chapter 11) in unpolarized case the strong Kohn’s anomaly $\text{Re} \sqrt{q - 2p_F}$ is ineffective for SC in the second order of perturbation theory for effective interaction $U_{\text{eff}}(q)$. However the situation is dramatically changed in spin-polarized case.

For $\alpha \neq 0$ in 2D:

$$\Pi_{\text{sing}}(q) \sim \text{Re} \sqrt{q_{\uparrow} - 2p_{F\downarrow}} \neq 0 \quad (12.1.13)$$

and thus Kohn’s anomaly is now “switched on” for SC already in the second order of the gas-parameter.

The exact calculation of $\Pi_{\downarrow\downarrow}(q)$ in 2D yields in p-wave channel (for magnetic number $m = 1$):

$$N_{\downarrow}^{2D} U_{eff}^{m=1} = 8f_0 \frac{\delta - 1}{\delta^2}, \quad (12.1.14)$$

where in 2D

$$\alpha = \frac{\delta^2 - 1}{\delta^2 + 1} \quad (12.1.15)$$

Correspondingly the critical temperature for p-wave pairing of two “up” spin reads in second order of 2D gas-parameter f_0 :

$$T_{C1}^{\uparrow\uparrow} \sim \varepsilon_F \exp\left\{-\frac{\delta^2}{8f_0(\delta-1)}\right\}, \quad (12.1.16)$$

From (12.1.16) we see that for $\delta = 0$ (unpolarized case) $T_{C1}^{\uparrow\uparrow} \rightarrow 0$ and superconductive transition arises only in third order of the gas-parameter for the effective interaction.

For $\alpha \rightarrow 1$ ($\delta \rightarrow \infty$) we again have $T_{C1}^{\uparrow\uparrow} \rightarrow 0$ in second order in f_0 .

Thus we have a very large maximum in between again. It corresponds to $\delta = p_{F\uparrow} / p_{F\downarrow} = 2$ or, $\alpha = 0.6$. Hence for $T_{C1}^{\uparrow\uparrow}$ in maximum we get:

$$\max T_{C1}^{\uparrow\uparrow} = T_{C1}^{\uparrow\uparrow}(\alpha = 0.6) \sim \varepsilon_F \exp\left\{-\frac{1}{2f_0^2}\right\}, \quad (12.1.17)$$

The dependence of $T_{C1}^{\uparrow\uparrow}$ from α in 2D spin-polarization Fermi-gas is shown on Fig.12.3.

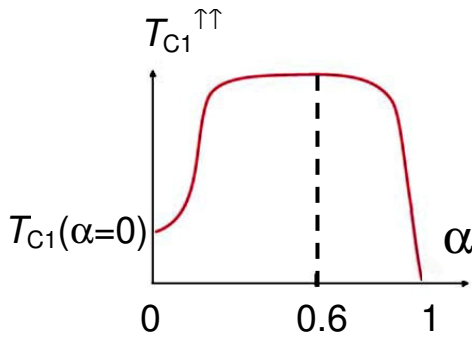


Fig.12.3. Dependence of the critical temperature $T_{C1}^{\uparrow\uparrow}$ for two “up” spins from the polarization degree α in 2D spin-polarized Fermi-gas.

The maximum is very broad in 2D – it stretches from $\alpha \sim 0.1$ till $\alpha \sim 0.9$.

Note that in this approximation (in second order in gas parameter evaluation of $T_{C1}^{\uparrow\uparrow}$) $T_{C1}^{\uparrow\uparrow}(\alpha = 1) = 0$ again due to the absence of “down” spins in 100% polarized case.

12.1.3. Spin-polarized superfluid ^3He .

The application of the theory for dilute spin-polarized mixture will be a subject of the next Chapter (Chapter 13). Here we would like to emphasize that even for dense superfluid ^3He (where $\lambda \sim 1.3$) we get reasonable estimates for $T_{C1}^{\uparrow\uparrow}$ - increase. These estimates are confirmed by the experiments of Frossati et al., [11.5] in Kamerlingh-Ohnes Laboratory in Leiden. Namely in unpolarized $^3\text{He-A}$:

$$T_{C1}(\alpha = 0) = 2.7 \text{ mK}. \quad (12.1.18)$$

In the same time for $\alpha = 6\%$ of the polarization (in magnetic fields ~ 15 T) $T_{C1}^{\uparrow\uparrow}(\alpha = 6\%) \approx 3.2$ mK and we have 20% increase of T_C .

In maximum for A1-phase of superfluid ^3He we predict

$$\max T_{C1}^{\uparrow\uparrow} = 6.4 T_{C1}^{\uparrow\uparrow}(\alpha = 0.6). \quad (12.1.19)$$

The similar estimate for reentrant behavior of $T_{C1}^{\uparrow\uparrow}(\alpha)$ and for $T_{C1}^{\uparrow\uparrow}$ in maximum was proposed in [12.6] on the basis of more phenomenological approach based on Landau Fermi-liquid theory for superfluid ^3He .

12.2. T_C enhancement in quasi-2D charged SC in parallel magnetic field.

In 2D electron gas in parallel magnetic field: $\vec{H} = H\vec{e}_x$ (see Fig.12.4) the vector-potential

$$\vec{A} = Hz\vec{e}_y \quad (12.2.1)$$

does not change the motion of electrons and Cooper pairs in (xy) plane (the Ψ -function for this problem $\Psi(\vec{r}) = e^{ip_x x + ip_y y} \varphi(z)$).

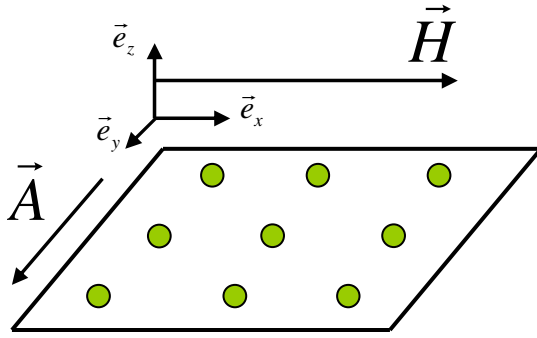


Fig.12.4. 2D electron gas in parallel magnetic field $\vec{H} = H\vec{e}_x$. Vector-potential $\vec{A} = Hz\vec{e}_y$ does not change the motion of electrons and Cooper pairs in (xy) plane.

Hence in this geometry diamagnetic Meissner effect [12.7] (which changes the motion of the Cooper pair in plane if magnetic field is perpendicular to the plane) is totally suppressed [12.9-12.11]. Hence 2D SC in parallel magnetic field becomes equivalent to neutral (uncharged) ^3He -monolayer and only Pauli paramagnetic effect is present [11.6]. According to this effect even if the singlet s-wave pairing organized by two electrons with spins “up” and “down” was present in SC at $H = 0$ it will be totally suppressed in magnetic fields exceeding Pauli paramagnetic limit [12.10,12.11]

$$H > H_p = \frac{T_{CO}}{g\mu_B}, \quad (12.2.2)$$

where μ_B is Bohr magneton and g is hyromagnetic ratio (or Lande factor) (note that for $T_{CO} \sim 1$ K and $g \sim 1$: $H_p \sim 1$ T). As a result only p-wave pairing with the symmetry of A1-phase (pairing of two electrons with spins “up”) that is with $S_{\text{tot}} = S_z^{\text{tot}} = 1$ survives in large magnetic field (the two electrons should lie on the same Fermi-surface with the radius $p_F\uparrow$).

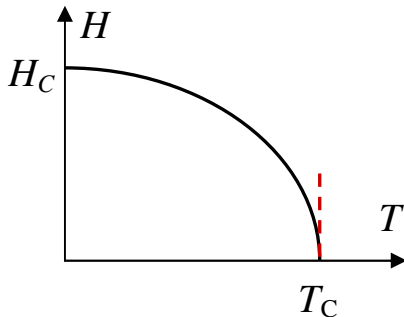


Fig.12.5. Standard behavior of a critical magnetic field as a function of temperature in 3D superconductors, which are subject of Meissner effect.

Hence instead of a standard behavior of a critical magnetic field H_C versus temperature [12.7] presented on Fig 12.5 we have very unusual (reentrant behavior) of p-wave critical temperatures in 2D superconductor in parallel magnetic field (see Fig.12.6).

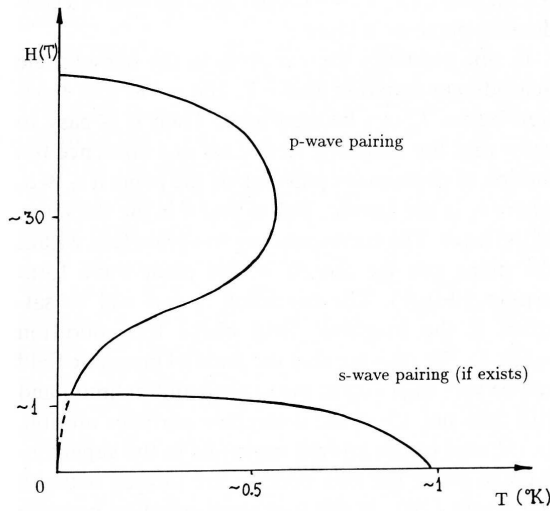


Fig.12.6. Suppression of s-wave pairing and reentrant behavior of p-wave critical temperatures in 2D SC in parallel magnetic field $H(T)$. p-wave pairing is formed by two electrons living on larger Fermi-surface (with $p_{F\uparrow}$) while effective interaction is formed by two electrons with down spins (with $p_{F\downarrow}$)

The critical temperature of p-wave pairing depends upon polarization degree according to (12.1.16). At small polarization degrees:

$$\alpha = \frac{g\mu_B H}{\mathcal{E}_{F0}} \ll 1 \quad (12.2.3)$$

in 2D case. For low density electron systems with $\mathcal{E}_F \sim 30$ K in high magnetic fields $H \sim 15$ T and $g \sim 1$ polarization degree $\alpha \sim 0.25$ and we can get $T_{C1}^{\uparrow\uparrow} \sim 0.5$ K in accordance with (12.1.16), (12.1.17) which is quite nice.

It is important to note that the results (12.1.16) and (12.1.17) are valid for 2D Fermi-gas with short-range repulsion or for 2D Hubbard model. The question is how these results will change in 2D Coulomb plasma (or 2D electron gas with screened Coulomb interaction). Here the coupling constant f_0 in (12.1.16) and (12.1.17) can be calculated only within accuracy of Random Phase

Approximation (RPA) for metallic electron densities with correlation radius $r_s \sim \frac{1}{p_F a_B} \gg 1$

($a_B = \frac{\mathcal{E}}{m^* e^2}$ is Bohr radius, m^* is effective mass and \mathcal{E} is effective dielectric permittivity)

[12.11, 12.13]. It is shown in [12.13] that in 2D electron gas (2DEG):

$$U_{\text{eff}}(q_{||} = 0) = \frac{\pi e^2}{\kappa_{TF}} \quad (12.2.4)$$

is 2D-projection of 3D screened Coulomb interaction. $\kappa_{TF} = 2\pi N_{2D}(0)e^2$ is Thomas-Fermi wave vector [12.11,12.13], $q_{||}$ is projection of vector \vec{q} on (xy) plane and $N_{2D}(0) = m/2\pi$ is a density of states in 2D.

The dimensionless coupling constant for screened Coulomb interaction reads:

$$f_0 = N_{2D}(0)U_{\text{eff}}(q=0) = \frac{m}{2\pi} \frac{\pi e^2}{\kappa_{TF}} = \frac{m}{2\pi} \frac{\pi e^2}{2\pi e^2 m / 2\pi} = \frac{1}{2} \quad (12.2.5)$$

- remarkable result which is valid also for 3D plasma where $N_{3D}(0) = m p_F / 2\pi^2$ and $U_{\text{eff}}(q=0) = \frac{4\pi e^2}{\kappa_{TF}^2}$. Thus effective gas-parameter for screened Coulomb plasma $f_0 = 1/2$ does not depend upon density both in 3D and 2D case.

Note that the RPA is exact in 3D and 2D for large densities and small correlation radius $r_s \ll 1$ (dense electron plasma considered in paragraph 11.5.1), but also it is not bad (at least in 3D) for standard metallic densities ($2 \leq r_s \leq 6$) because the effective parameter of expansion in the energy-functional of 3D electron plasma is actually $\sim r_s/6$ (see [12.11, 11.49, 11.50]). We can hope that (12.1.16) and (12.1.17) with $f_0 \sim 1/2$ provides qualitative estimates for 2D dense electron plasma.

Note that the most important experimental limitation to this scenario is connected with the demands on the purity of the sample. In accordance with Abrikosov-Gor'kov results for paramagnetic impurities (more exactly Gor'kov, Larkin results for non-magnetic impurities in p-wave SC) it means that for inverse scattering time:

$$\gamma = 1/\tau < T_{C1} \quad (\hbar = k_B = 1). \quad (12.2.6)$$

For $T_C \sim 0.5$ K we get then $\tau \geq 2 \cdot 10^{-11}$ see for scattering time of electrons on impurities. Accordingly in 2D case the sheet conductivity for $\varepsilon_F \sim 30$ K and $T_C \sim 0.5$ K:

$$\sigma_{\square} > \frac{e^2}{2\pi\hbar} \frac{2\varepsilon_F}{T_C} \sim 120 \frac{e^2}{2\pi\hbar}. \quad (12.2.7)$$

Hence plaquette resistance:

$$R_{\square} < \frac{1}{120} \frac{2\pi\hbar}{e^2} \sim 0.2 \text{ k}\Omega \quad (12.2.8)$$

and mobility:

$$\mu_{el} = \frac{e\tau}{m^*} = 3 \cdot 10^4 \left(\frac{m_e}{m^*} \right) \text{ cm}^2 \text{ V}^{-1} \text{ s}^{-1} \quad (12.2.9)$$

Thus for semimetals or degenerate 2D semiconductive layers with light effective mass $m^* \sim 0.1 m_e$ (heterostructures, inverse layers):

$$\mu_{el} = 10^5 \text{ cm}^2 \text{ V}^{-1} \text{ s}^{-1}, \quad (12.2.10)$$

which requires very clean samples.

Note that the highest mobility for GaAs-AlAs heterostructures utilized for the measurements of Fractional Quantum Hall effect $\mu_{el} \sim 10^7$. In these systems $\varepsilon_F \sim 30$ K for densities $n_{2D} \sim 10^{12} \text{ cm}^{-2}$, Bohr radius $a_B = \varepsilon / m^* e^2$ with effective dielectric permittivity $\varepsilon \sim 4$. Thus the correlation radius $r_s \sim 4$, so we are far from Wigner crystal case ($r_s \sim 20$ in 2D) [12.11, 12.13] and can hope that RPA theory works quite well also in 2D for these densities. Thus we can justify the estimates for $T_{C1}^{\uparrow\uparrow}$ with $f_0 = 1/2$ (12.1.16) and (12.1.17) for heterostructures.

Note that if we consider 2D organic superconductors like α -(BEDT-TTF)₂I₃ or intercalated systems (dichalcogenides) TaS₂, TaSe₂ then their mobilities are also very high, but they have Fermi-energies $\varepsilon_F \sim (10^3 \div 10^4)$ K which are very difficult to polarize even with very high magnetic fields (maximal possible stationary magnetic fields are equal to 30 T, maximal fields in pulsed regime are 100 T today, hence polarization degree $\alpha = \frac{g\mu_B H}{\varepsilon_{F0}}$ will be very low and T_{C-s} will be low).

If we start to think about 2D layer of p-wave heavy-fermion SC like UBe₁₃ with $m^* \sim 200 m_e$ and $\varepsilon_F \sim (30 \div 50)$ K, than we should realize that it is very difficult now to grow very thin films of high quality and it is necessary also to take into account strong spin-orbital coupling and the influence of the crystalline fields in these substances.

It is a very nice challenge for experimentalists to grow very good quality 2D-samples and to apply very parallel magnetic fields or to change gradually tilting angle for a field from $\pi/2$ to 0 and measure an appearance of p-wave SC at very small angles (note that already very small perpendicular component of the magnetic field will destroy SC via diamagnetic Meissner effect). In the end of this section let us mention that in principle a reentrant behavior of T_C from magnetic field (similar to the one shown on Fig.12.6) can be realized even in 3D superconductors in so-called superquantum limit [12.14, 12.15]. This limit corresponds to very high magnetic fields and very small Fermi-energies when Larmor frequency $\omega_L \sim \mu_B H > \varepsilon_F$ (note that $\varepsilon_F \gg T_C$). In this situation we should take into account Landau quantization of electron levels in magnetic field (diamagnetic one-particle effect). Moreover for $\omega_L > \varepsilon_F$ only one Landau level is filled, so the spectrum of electrons becomes quasi one-dimensional $\varepsilon(p) = \frac{\hbar \omega_L}{2} + \frac{p_z^2}{2m}$ and we again have parquette situation with the necessity to sum up an infinite number of diagrams for effective interaction U_{eff} in particle-particle and particle-hole channels. Halperin and Tesanovic [12.15] showed that as a result a reentrant behavior takes place (the SC appears again in very high fields).

12.3.Strong T_C enhancement in the two-band SC.

Another possibility to enhance the critical temperature of p-wave pairing is to consider the two-band model with two sorts of fermions. The main idea again is that to separate the channels: the two particles of sort 1 form the Cooper channel (for $p_{F1} > p_{F2}$), then the effective interaction is formed by two particles of sort 2 (see Fig.12.7).

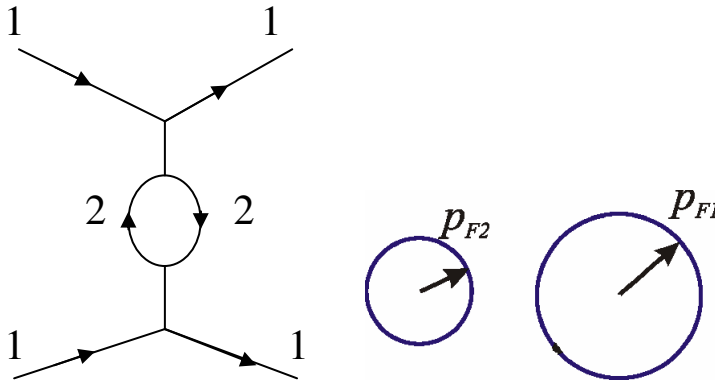


Fig.12.7. Effective interaction for two sorts of particles with $p_{F1} > p_{F2}$.

In this case all the results of section (12.1) are valid with the change of $\delta = p_{F\uparrow} / p_{F\downarrow}$ on $\delta = p_{F1} / p_{F2}$. The gas-parameters λ and f_0 now depend upon the interaction between the particles of sort 1 and sort 2. In the simplest case it reads $\frac{U_{12}}{2} \sum_i n_{1i} n_{2i}$, where U_{12} is interband interaction, n_{1i} and n_{2i} are the densities of the particles with sort 1 and 2 on site i .

Let us consider the physics which appears in the two-band model for the most interesting case of very different masses of the two sorts of fermions.

12.3.1. The two-band Hubbard model with one narrow band.

On the lattice the most general and simple model which describes this situation is the two-band Hubbard model with one narrow band. This model is very rich. It describes adequately mixed valence systems [12.16, 12.17] such as uranium based heavy-fermions and also some other novel

SC and transition metal systems with orbital degeneracy such as complex magnetic oxides (CMR systems) in optimally doped case. Moreover it contains such highly nontrivial effect as electron-polaron effect [12.18, 12.19] in the homogeneous case. It also shows the tendency towards phase separation [12.20] for a large mismatch between the densities of heavy and light bands as well as anomalous resistivity characteristics (we will study them in the next chapters). In addition to that it describes anomalous p-wave SC of enhanced Kohn-Luttinger type which we will study detaily in this paragraph. The Hamiltonian of the two-band Hubbard model in real space reads:

$$\begin{aligned}\hat{H}' = & -t_h \sum_{\langle ij \rangle \sigma} a_{i\sigma}^+ a_{j\sigma} - t_L \sum_{\langle ij \rangle \sigma} b_{i\sigma}^+ b_{j\sigma} - \varepsilon_0 \sum_{i\sigma} n_{ih}^\sigma - \mu \sum_{i\sigma} (n_{i\sigma}^L + n_{i\sigma}^h) + \\ & + U_{hh} \sum_i n_{ih}^\uparrow n_{ih}^\downarrow + U_{LL} \sum_i n_{iL}^\uparrow n_{iL}^\downarrow + \frac{U_{hL}}{2} \sum_i n_{iL} n_{ih}\end{aligned}\quad (12.3.1)$$

where t_h and t_L are hopping integrals in heavy and light bands, $-\varepsilon_0$ is the center of gravity of the heavy band, and the difference Δ between the bottoms of the bands is given by:

$$\Delta = -\varepsilon_0 + \frac{W_L - W_h}{2} = E_{\min}^h - E_{\min}^L \quad (12.3.2)$$

U_{hh} and U_{LL} are intraband Hubbard interactions for heavy and light electrons, U_{hL} is interband Hubbard interaction for heavy and light electrons, $n_{ih}^\sigma = a_{i\sigma}^+ a_{i\sigma}$, $n_{iL}^\sigma = b_{i\sigma}^+ b_{i\sigma}$ are the densities of heavy and light electrons on site i with spin-projection σ , μ is chemical potential.

After Fourier transformation we obtain:

$$\begin{aligned}\hat{H}' = & \sum_{\vec{p}\sigma} [\varepsilon_h(p) - \mu] a_{p\sigma}^+ a_{p\sigma} + \sum_{\vec{p}\sigma} [\varepsilon_L(p) - \mu] b_{p\sigma}^+ b_{p\sigma} + U_{hh} \sum_{\vec{p}\vec{p}'\vec{q}} a_{\vec{p}\uparrow}^+ a_{\vec{p}\downarrow}^+ a_{\vec{p}-\vec{q}\downarrow} a_{\vec{p}'+\vec{q}\uparrow} + \\ & + U_{LL} \sum_{\vec{p}\vec{p}'\vec{q}} b_{\vec{p}\uparrow}^+ b_{\vec{p}\downarrow}^+ b_{\vec{p}-\vec{q}\downarrow} b_{\vec{p}'+\vec{q}\uparrow} + \frac{U_{hL}}{2} \sum_{\substack{\vec{p}\vec{p}'\vec{q} \\ \sigma\sigma'}} a_{\vec{p}\sigma}^+ (b_{\vec{p}'\sigma'}^+ b_{\vec{p}-\vec{q}\sigma'}) a_{\vec{p}'+\vec{q}\sigma},\end{aligned}\quad (12.3.3)$$

where in D dimensions ($D = 2, 3$) for the hypercubic lattice:

$$\varepsilon_h(p) - \mu = -2t_h \sum_{a=1}^D \cos(p_a d) - \varepsilon_0 - \mu, \quad (12.3.4)$$

and

$$\varepsilon_L(p) - \mu = -2t_L \sum_{a=1}^D \cos(p_a d) - \mu, \quad (12.3.4)$$

are the uncorrelated quasiparticle energies for heavy and light bands (see Fig.12.8) and $p_a = \{p_x, p_y, \dots\}$ are Cartesian projections of the momentum.

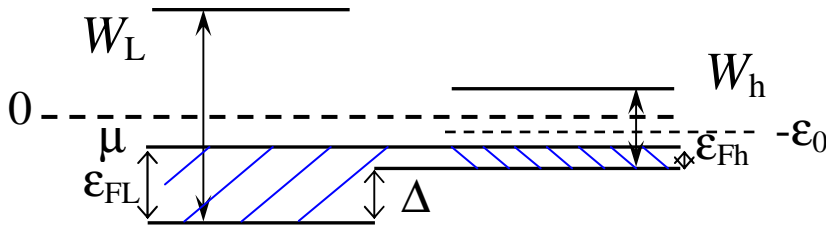


Fig.12.8. Band structure in the two-band model with one narrow band. W_h and W_L are the bandwidths of heavy and light electrons, ε_{Fh} and ε_{Fh} are the Fermi-energies,

$\Delta = -\varepsilon_0 + \frac{W_L - W_h}{2} = E_{\min}^h - E_{\min}^L$ is the energy difference between the bottoms of the heavy and

light bands, with $(-\varepsilon_0)$ being the center of gravity of the heavy band. The center of gravity of the light band is zero, μ is chemical potential.

For low densities of heavy and light components $n_{\text{tot}}d^D = (n_h + n_L) d^D \ll 1$, the quasiparticle spectra are:

$$\begin{aligned}\varepsilon_h(p) - \mu &= -\frac{W_h}{2} + t_h(p^2 d^2) - \varepsilon_0 - \mu, \\ \varepsilon_L(p) - \mu &= -\frac{W_L}{2} + t_L(p^2 d^2) - \mu\end{aligned}\quad (12.3.5)$$

where $W_h = 4Dt_h$ and $W_L = 4Dt_L$ are bandwidths of heavy and light electrons for D - dimensional hypercubic lattice (for $D = 3$ we have $W_h = 12t_h$ and $W_L = 12t_L$, for $D = 2$ the bandwidths read $W_h = 8t_h$ and $W_L = 8t_L$).

Introducing again (as in one-band Hubbard model in section 11.4) the bare masses of heavy and light components:

$$m_h = \frac{1}{2t_h d^2}; m_L = \frac{1}{2t_L d^2} \quad (12.3.6)$$

and Fermi-energies:

$$\varepsilon_{Fh} = \frac{p_{Fh}^2}{2m_h} = \frac{W_h}{2} + \mu + \varepsilon_0, \quad \varepsilon_{FL} = \frac{p_{FL}^2}{2m_L} = \frac{W_L}{2} + \mu \quad (12.3.7)$$

we finally obtain uncorrelated quasiparticle spectra (for temperatures $T \rightarrow 0$) as:

$$\varepsilon_h(p) - \mu = \frac{p^2}{2m_h} - \varepsilon_{Fh}, \quad \varepsilon_L(p) - \mu = \frac{p^2}{2m_L} - \varepsilon_{FL} \quad (12.3.8)$$

In deriving (12.3.5) - (12.3.8) we implicitly assumed that the difference between the bottoms of the heavy and light bands Δ on Fig.12.8 is not too large, and hence the parabolic approximation for the spectra of both bands is still valid. We note that there is no one-particle hybridization in Hamiltonians (12.3.1), (12.3.3) but there is a strong two particle hybridization

$\frac{U_{hL}}{2} \sum_i n_i^h n_i^L$ connected with interband Hubbard interaction $U_{12} = U_{hL}$.

We assume that $m_h \gg m_L$ and therefore:

$$W_h/W_L = m_L/m_h \ll 1 \quad (12.3.9)$$

We also assume that the strong-coupling situation $U_{hh} \sim U_{LL} \sim U_{hL} \gg W_L \gg W_h$ takes place (note that U_{hL} is large because in reality light particles experience strong scattering on the heavy ones as if on a quiresonance level).

Finally throughout this Chapret we will consider the simplest case where the densities of the

bands are of the same order: $n_h \sim n_L \sim n$ (where in 3D $n = \frac{p_F^3}{2\pi^2}$, and in 2D $n = \frac{p_F^2}{2\pi}$). In the end

of this section note that the two-band Hubbard model with one narrow band is natural generalization of the well-known Falikov-Kimball model with one finite mass and one infinitely large mass[12.21] but contains much more rich physics due to a finite width of a heavy band (instead of a localized level in [12.21]) which allows an interesting dynamics of the heavy component.

12.3.2. The Kanamori T-matrix approximation.

In Chapter 11 (section 12.4) when we discussed SC in 3D and 2D one-band Hubbard model at low density we already acquainted ourselves with Kanamori T-matrix approximation [11.33]. Let us apply the same scheme for a two-band Hubbard model. In the 3D case the solution of the corresponding Lipman-Shwinger equations [11.35] yield (see Fig.12.9):

$$T_{hh} = \frac{U_{hh}d^3}{(1 - U_{hh}d^3 K_{hh}^{vac}(0,0))} \approx \frac{U_{hh}d^3}{\left(1 + \frac{U_{hh}}{8\pi t_h}\right)}; \quad (12.3.10)$$

$$T_{hL} \approx \frac{U_{hL}d^3}{\left(1 + \frac{U_{hL}}{8\pi t_{hL}^*}\right)}; \quad T_{LL} = \frac{U_{LL}d^3}{\left(1 + \frac{U_{LL}}{8\pi t_L}\right)},$$

where $K_{hh}^{vac}(0,0) = - \int_0^{1/d} \frac{d^3 \vec{p}}{(2\pi)^3} \frac{m_h}{p^2}$ is a Cooper loop for heavy particles in vacuum, the effective hopping integrals

$$t_{hL}^* = \frac{1}{2d^2 m_{hL}^*} \text{ and } m_{hL}^* = \frac{1}{2t_{hL}d^2} = \frac{m_h m_L}{(m_h + m_L)} \approx m_L \quad (12.3.11)$$

is an effective mass for T-matrix T_{hL} for $m_h \gg m_L$ (note that T-matrix T_{hL} describes scattering of heavy electrons on the light ones).

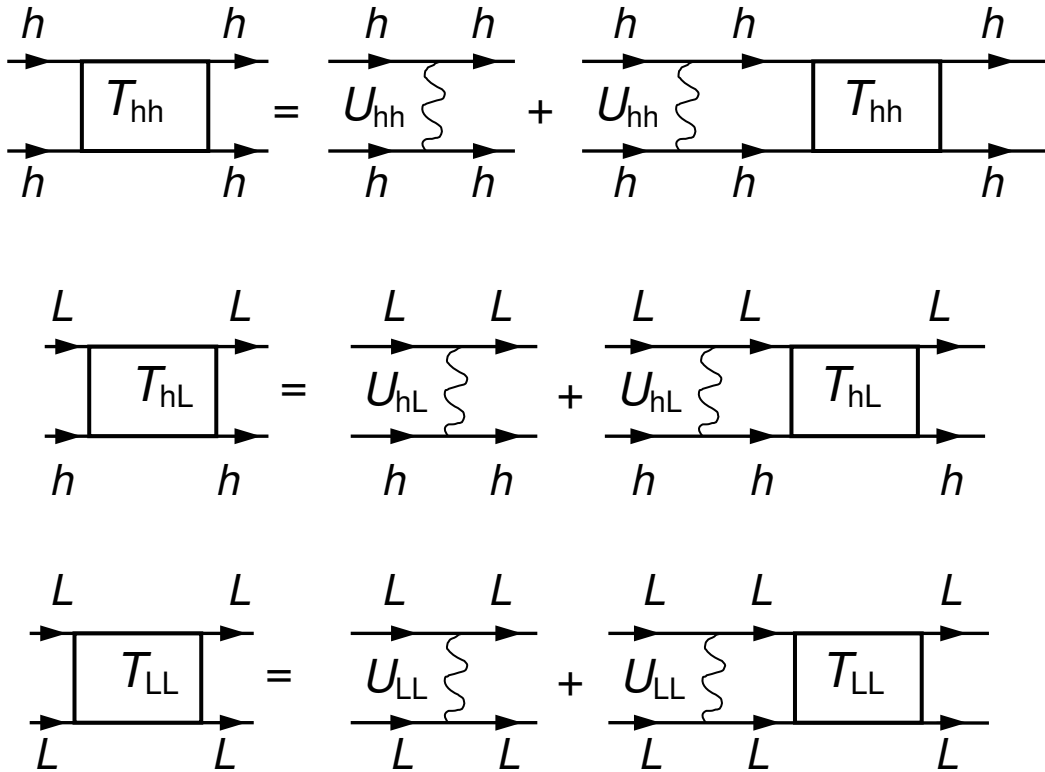


Fig.12.9. Lipman-Schwinger equations for T-matrices T_{hh} , T_{LL} and T_{hL} for the two-band model with heavy (h) and light (l) electrons, U_{hh} and U_{LL} are the intraband Hubbard interactions, U_{hL} is the interband Hubbard interaction between heavy and light particles.

Accordingly $t_{hL}^* \sim t_L$ is an effective hopping integral for this T-matrix. The quantities $U_{hh}d^3$, $U_{hL}d^3$ and $U_{LL}d^3$ play the role of zeroth Fourier components for the intraband and interband Hubbard interactions U_{hh} , U_{hL} and U_{LL} in 3D. As a result in the strong-coupling case for $U_{hh} \sim U_{LL} \sim U_{hL} \gg W_L \gg W_h$ we have:

$$T_{hh} \approx 8\pi t_h d^3; \quad T_{hL} \approx T_{LL} \approx 8\pi t_L d^3 \quad (12.3.12)$$

The s-wave scattering lengths for the two-band Hubbard model $a = \frac{mT}{4\pi} = \frac{T}{8\pi t d^2}$ then read in the strong-coupling case:

$$a_{hh} = a_{hL} = a_{LL} = d \quad (12.3.13)$$

Correspondingly, the gas-parameter of Galitskii $\lambda = 2a p_F/\pi$ in the case of equal densities of heavy and light bands $n_h = n_L$ is given by:

$$\lambda = \left(\lambda_L \approx \frac{2dp_{FL}}{\pi} \right) = \left(\lambda_h \approx \frac{2dp_{Fh}}{\pi} \right) = \frac{2dp_F}{\pi} \quad (12.3.14)$$

In the 2D case for strong Hubbard interactions and low densities the vacuum T-matrices for $n_h = n_L$ with logarithmic accuracy are given by:

$$T_{hh} \approx \frac{U_{hh}d^2}{\left(1 + \frac{U_{hh}d^2}{8\pi t_h} \int_{-1/p_F}^{-1/d^2} \frac{dp^2}{p^2} \right)} \approx \frac{U_{hh}d^2}{1 + \frac{U_{hh}}{8\pi t_h} \ln \frac{1}{p_F^2 d^2}}; \quad (12.3.15)$$

$$T_{LL} = \frac{U_{LL}d^2}{1 + \frac{U_{LL}}{8\pi t_L} \ln \frac{1}{p_F^2 d^2}}; \quad T_{hL} = \frac{U_{hL}d^2}{1 + \frac{U_{hL}}{8\pi t_{hL}^*} \ln \frac{1}{p_F^2 d^2}},$$

where Ud^2 plays the role of zeroth Fourier component of the Hubbard potential in 2D. As a result, in the strong-coupling case, the 2D gas-parameter of Bloom [11.3] for equal densities $n_h = n_L$ reads:

$$f_0 = f_{0L} = f_{0h} = \frac{1}{2 \ln \frac{1}{p_F d}}. \quad (12.3.16)$$

12.3.3. Evaluation of the self-energies of heavy and light bands

Let us now evaluate the self-energies of heavy and light bands. In the two-band model the self-energies of heavy and light particles read (see Fig.12.10):

$$\Sigma_h = \Sigma_{hh} + \Sigma_{hL} \text{ and } \Sigma_L = \Sigma_{LL} + \Sigma_{Lh}. \quad (12.3.17)$$

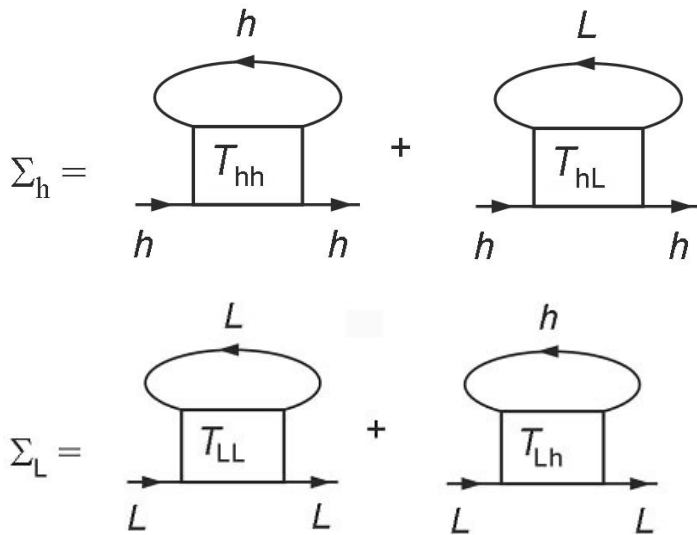


Fig.12.10. The self-energies of heavy and light particles in the T-matrix approximation. T_{hh} , T_{LL} , T_{Lh} , and T_{hL} are full T-matrices of heavy and light particles in substance.

In 3D case the full T-matrices T_{hh} in substance which enter in the first diagram for Σ_h in Fig. 12.10 has the form:

$$T_{hh}(\Omega, \vec{p}) = \frac{U_{hh}d^3}{(1 - U_{hh}d^3K_{hh}(\Omega, \vec{p}))}, \quad (12.3.18)$$

where according to [12.4, 11.34]:

$$K_{hh}(\Omega, \vec{p}) = \int \frac{d^3\vec{p}'}{(2\pi)^3} \frac{(1 - n_h^F(\varepsilon_{\vec{p}'+\vec{p}} - \mu) - n_h^F(\varepsilon_{-\vec{p}'} - \mu))}{(\Omega - \varepsilon_h(\vec{p}'+\vec{p}) - \varepsilon_h(-\vec{p}') + 2\mu + i0)} - \quad (12.3.19)$$

is a Cooper loop in substance (the product of the two Green's functions in the Cooper (particle-particle) channel), $n_h^F(\varepsilon - \mu)$ is the Fermi - Dirac distribution function for heavy particles, and similarly for the full T-matrices T_{hL} , T_{Lh} and T_{LL} and Cooper loops K_{hL} , K_{Lh} and K_{LL}

If we expand the T-matrix for heavy particles in first two orders in the gas-parameter, than according to Galitskii [11.2] we obtain:

$$T_{hh}(\Omega, \vec{p}) = \frac{4\pi a_h}{m_h} + \left(\frac{4\pi a_h}{m_h}\right)^2 (K_{hh} - K_{hh}^{vac}) + o\left[\left(\frac{4\pi a_h}{m_h}\right)^3 (K_{hh} - K_{hh}^{vac})^2\right], \quad (12.3.20)$$

where

$$\frac{4\pi a_h}{m_h} \approx \frac{U_{hh}d^3}{(1 - U_{hh}d^3K_{hh}^{vac})} \quad (12.3.21)$$

coincides with the Kanamori approximation for the vacuum T-matrix and

$$K_{hh}^{vac}(\Omega, \vec{p}) = \int \frac{d^3\vec{p}'/(2\pi)^3}{\left(\Omega - \frac{(\vec{p}'+\vec{p})^2}{2m_h} - \frac{p'^2}{2m_h}\right)} \quad (12.3.22)$$

is the Cooper loop in vacuum (rigorously speaking the scattering length is defined by $K_{hh}^{vac}(0,0)$, but the difference between $K_{hh}^{vac}(\Omega, \vec{p})$ and $K_{hh}^{vac}(0,0)$ is proportional to the gas-parameter $a_h p_{Fh}$ and is small). K_{hh} in (12.3.20) is the full Cooper loop (cooperon) in substance for heavy particles given by (12.3.19). If we consider the low densities and the energies close to ε_F we can show that the terms neglected in T_{hh} are small with respect to the gas-parameter

$$\frac{4\pi a_h}{m_h} (K_{hh} - K_{hh}^{vac}) \sim a_h p_{Fh}. \quad (12.3.23)$$

The self-energy of heavy particles Σ_{hh} in the first two orders of the gas-parameter is given by:

$$\Sigma_{hh}(p) = \sum_k T_{hh}(k+p)G_h(k) \approx \frac{4\pi a_h}{m_h} \sum_k G_h(k) - \left(\frac{4\pi a_h}{m_h}\right)^2 \sum_k (K_{hh} - K_{hh}^{vac})G_h(k) + o(a_h p_{Fh})^3. \quad (12.3.24)$$

The first term becomes $\frac{4\pi a_h}{m_h} n_h$ which is just the Hartree-Fock contribution [11.2, 11.19]. In the

second term we can make an analytic continuation $i\omega_n \rightarrow \omega + i0$ for bosonic propagator K_{hh} and fermionic propagator G_h [12.22, 12.23]. As a result (bearing in mind that $\text{Im} K_{hh}^{vac} = 0$) we

obtain the imaginary part of $\Sigma_{hh}^{(2)}$ as:

$$\begin{aligned} \text{Im} \Sigma_{hh}^{(2)}(\varepsilon, \vec{p}) &= \left(\frac{4\pi a_h}{m_h}\right)^2 \sum_k \text{Im} K_{hh}(\varepsilon_k + \varepsilon - \mu, \vec{k} + \vec{p}) [n_B(\varepsilon_k + \varepsilon - \mu) + n_F(\varepsilon_k - \mu)] = \\ &= -\left(\frac{4\pi a_h}{m_h}\right)^2 \pi \int \frac{d^3\vec{k}}{(2\pi)^3} \int \frac{d^3\vec{p}'}{(2\pi)^3} [1 - n_h^F(\vec{p} + \vec{p}' + \vec{k}) - n_h^F(-\vec{p}')] [n_B(\varepsilon_k + \varepsilon - \mu) + n_F(\varepsilon_k - \mu)] \cdot \\ &\cdot \delta[\varepsilon + \varepsilon_h(\vec{k}) - \varepsilon_h(\vec{p} + \vec{p}' + \vec{k}) - \varepsilon_h(-\vec{p}') + \mu] \end{aligned} \quad (12.3.25)$$

and similarly for the real part of $\Sigma_{hh}^{(2)}$:

$$\text{Re}\Sigma_{hh}^{(2)}(\varepsilon, \vec{p}) = \left(\frac{4\pi a_h}{m_h}\right)^2 \sum_k \left[\text{Re}K_{hh}(\varepsilon_k + \varepsilon - \mu, \vec{k} + \vec{p}) - \text{Re}K_{hh}^{vac}(\varepsilon_k + \varepsilon_p - 2\mu, \vec{k} + \vec{p}) \right] [n_B(\varepsilon_k + \varepsilon - \mu) + n_F(\varepsilon_k - \mu)] \quad (12.3.26)$$

where for the real part of a Cooper loop in vacuum we have:

$$\text{Re}K_{hh}^{vac}(\varepsilon_k + \varepsilon_p, \vec{k} + \vec{p}) = \int \frac{d^3 \vec{p}'}{(2\pi)^3} P \frac{2m_h}{\vec{k}^2 + \vec{p}^2 - (\vec{p}' + \vec{k} + \vec{p})^2 - \vec{p}'^2} \quad (12.3.27)$$

Thus $\text{Re}K_{hh}^{vac}$ is calculated in resonance for $\Omega = \varepsilon_k + \varepsilon_p$ (or for $\varepsilon = \varepsilon_p$), where P is the principal value. In (12.3.25) and (12.3.26) $n_B(\Omega) = \frac{1}{(e^{\Omega/T} - 1)}$ and $n_F(\Omega) = \frac{1}{(e^{\Omega/T} + 1)}$ are the bosonic and fermionic distribution functions and hence:

$$n_B(\varepsilon_k + \varepsilon - \mu) + n_F(\varepsilon_k - \mu) = \frac{1}{2} \left[\text{cth} \frac{(\varepsilon_k + \varepsilon) - \mu}{2T} + \text{th} \frac{\varepsilon_k - \mu}{2T} \right] \quad (12.3.28)$$

The real part of a Cooper loop in substance for heavy particles is given by:

$$\text{Re}K_{hh}(\varepsilon_k + \varepsilon - \mu, \vec{k} + \vec{p}) = \int \frac{d^3 \vec{p}'}{(2\pi)^3} \frac{[1 - n_h^F(\vec{p} + \vec{p}' + \vec{k}) - n_h^F(-\vec{p}')] }{[\varepsilon + \varepsilon_h(\vec{k}) - \varepsilon_h(\vec{p} + \vec{p}' + \vec{k}) - \varepsilon_h(-\vec{p}') + \mu]} \quad (12.3.29)$$

The analytic continuation for $\Sigma_{hh}^{(2)}$ in a 2D case is similar to the one in the 3D case.

We note that for $\Omega/T \gg 1$, the bosonic distribution function $n_B(\Omega) \rightarrow 0$ and the fermionic distribution function $n_F(\Omega) \rightarrow \theta(\Omega)$ - to the step-function. Hence at low temperatures $\text{Im}\Sigma_{hh}$ and $\text{Re}\Sigma_{hh}$ acquire the standard form [11.2, 11.19, 11.20]. We will analyze their behavior at finite temperatures more detailly in Chapters 16 and 17.

Note that for higher temperatures we should keep in mind that $n_B(\Omega) \rightarrow T/\Omega$ for $T \gg \Omega$. The fermionic distribution function is “washed out” by temperature. Accordingly, $n_B(\Omega) = \frac{1}{2} \left(1 - \frac{\Omega}{2T} \right)$. These approximations are important when we evaluate $\text{Im}\Sigma$ for higher temperatures $T > W_h$ [11.32] in chapter 17.

We note that in contrast with the model of slightly non-ideal Fermi-gas (see [11.2, 11.19, 11.20]) the Hubbard model does not contain an exchange-type diagram for Σ_{hh} (see Fig. 12.11) because the T-matrix in this diagram corresponds to incoming and outgoing heavy particles with the same spin-projection $a_\sigma^\dagger a_\sigma^\dagger a_\sigma a_\sigma$ while the Hubbard model contains only the matrix elements $a_\uparrow^\dagger a_\downarrow^\dagger a_\downarrow a_\uparrow$ with different spin-projections.

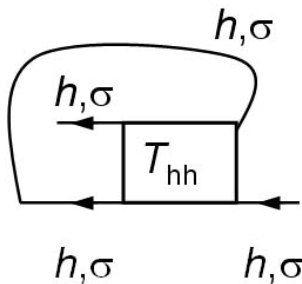


Fig. 12.11. An exchange – type diagram for the self-energy Σ_{hh}^σ which contains the matrix element $a_\sigma^\dagger a_\sigma^\dagger a_\sigma a_\sigma$ and thus is absent in the Hubbard model.

We also note that when we expand the T-matrix up to second order in the gas-parameter, we implicitly assume that the T-matrix itself does not have a simple pole structure of the type of a bosonic propagator. This is a case for a partially filled heavy band $n_h d^D \ll 1$ and the low energy sector where $0 < \varepsilon < W_h \ll U_{hh}$. Effectively we neglect the lattice in this expansion. However if we take the lattice into account, then we will get two poles for the full (unexpanded) T-matrix of heavy particles in (12.3.18). The first one is connected with the so-called antibound

state predicted by Hubbard [11.29] and Anderson [12.24] and corresponds to large positive energy:

$$\varepsilon \sim U_{hh} > 0 \quad (12.3.30)$$

Physically it describes an antibound pair of two heavy particles with energy of U_{hh} on the same lattice site. It therefore reflects the presence of the upper Hubbard band already at low densities $n_h d^D \ll 1$ [12.25]. But we will show that the intensity of the upper Hubbard band (UHB) is small at low densities and for low energy sector. The more detailed discussion of the antibound state will be a subject of Chapter 16.

A second pole in the full T-matrix found by [12.26] corresponds to negative energy and in the 2D case yields:

$$\varepsilon \approx -2\varepsilon_{Fh} - \frac{2\varepsilon_{Fh}^2}{W_h} < 0 \quad (12.3.31)$$

It describes the bound state of the two holes below the bottom of the heavy band ($\varepsilon < -2\varepsilon_{Fh}$). Therefore, it has zero imaginary part and does not contribute to $\text{Im}T$. (This mode produces non-analytic corrections to $\text{Re}\Sigma_{hh} \sim |\varepsilon|^{5/2}$ in 2D). We will also consider this mode more detailly in Chapter 16. In the forthcoming sections we can neglect both these two contributions to the T-matrices and self-energies.

12.3.4. Electron polaron effect.

For temperatures $T \rightarrow 0$ the one-particle Green's functions for heavy and light electrons are given by [11.19, 11.20]:

$$G_h(\omega, \vec{q}) = \frac{1}{(\omega - \varepsilon_h(q) + \mu - \Sigma_h(\omega, \vec{q}))} \approx \frac{Z_h}{(\omega - \varepsilon_h^*(q) + \mu + i0)} \quad (12.3.32)$$

and respectively

$$G_L(\omega, \vec{q}) \approx \frac{Z_L}{(\omega - \varepsilon_L^*(q) + \mu + i0)}, \quad (12.3.33)$$

where according to Galitskii [11.2]:

$$\varepsilon_h^*(q) - \mu = \frac{(q^2 - p_{Fh}^2)}{2m_h^*} \quad \text{and} \quad \varepsilon_L^*(q) - \mu = \frac{(q^2 - p_{FL}^2)}{2m_L^*} \quad (12.3.34)$$

are renormalized quasiparticle spectra, and

$$Z_h^{-1} = \left(1 - \frac{\partial \text{Re}\Sigma_h^{(2)}(\omega, \vec{q})}{\partial \omega} \bigg|_{\substack{\omega \rightarrow 0 \\ q \rightarrow p_{Fh}}} \right); \quad Z_L^{-1} = \left(1 - \frac{\partial \text{Re}\Sigma_L^{(2)}(\omega, \vec{q})}{\partial \omega} \bigg|_{\substack{\omega \rightarrow 0 \\ q \rightarrow p_{FL}}} \right) - \quad (12.3.35)$$

are inverse Z-factors [11.20, 11.19, 12.27, 12.28] of heavy and light electrons. The leading contribution to $\text{Im}\Sigma_h^{(2)}$ in (12.3.35) comes from the substitution of $\text{Re}\Sigma_{hL}^{(2)}(\omega, \vec{q})$ to Z_h^{-1} , which is described by a formula similar to (12.3.26), and yields:

$$\begin{aligned} 1 - Z_h^{-1} &= \lim_{\substack{\omega \rightarrow 0 \\ q \rightarrow p_{Fh}}} \frac{\partial \text{Re}\Sigma_{hL}^{(2)}(\omega, \vec{q})}{\partial \omega} \sim - \left(\frac{4\pi a_{hL}}{m_{hL}^*} \right)^2 \iint \frac{d^D \vec{p}}{(2\pi)^D} \frac{d^D \vec{p}'}{(2\pi)^D} \cdot \\ &\cdot \frac{[1 - n_L^F(\vec{p}' + \vec{p}) - n_h^F(-\vec{p}')] n_L^F(\vec{p} - \vec{q})}{[\varepsilon_L(\vec{p} - \vec{q}) - \varepsilon_L(\vec{p}' + \vec{p}) - \varepsilon_h(-\vec{p}') + \mu]^2}, \end{aligned} \quad (12.3.36)$$

where $n_B(\Omega) \rightarrow 0$, $n_F(\Omega)$ is a step function for $\Omega/T \gg 1$; $a_{hL} \approx d$ in 3D is connected with the vacuum T-matrix T_{hL} , and $m_{hL}^* \approx m_L$. Replacing in (12.3.36) $\frac{d^D \vec{p}}{(2\pi)^D} \frac{d^D \vec{p}'}{(2\pi)^D}$ by

$N_L^2(0)d\epsilon_L(\vec{p})d\epsilon_L(\vec{p}')$ (where $N_L(0)$ is a density of states of light particles, $D = 2, 3$), and taking into account that in (12.3.36) $\epsilon_L(\vec{p} - \vec{q}) - \mu < 0$ while $\epsilon_L(\vec{p}' + \vec{p}) - \mu > 0$ we can easily verify that for $m_h \gg m_L$ or equivalently for $\epsilon_{FL} \gg \epsilon_{Fh}$ this expression contains a large logarithm both in 3D and 2D cases (see [12.18]). Hence, the Z-factor of the heavy particles in 3D in the leading approximation in the gas-parameter $\lambda = 2a p_F/\pi$ is given by:

$$Z_h^{-1} \approx 1 + 2\lambda^2 \ln \frac{m_h}{m_L} \quad (12.3.37)$$

Correspondingly, in 2D:

$$Z_h^{-1} = 1 + 2f_0^2 \ln \frac{m_h}{m_L} \quad (12.3.38)$$

where $f_0 = \frac{1}{2 \ln(1/p_{FL}d)}$ - 2D gas-parameter of Bloom.

We note that the contribution to Z_h^{-1} from $\text{Re}\Sigma_{hh}^{(2)}$ does not contain a large logarithm and thus is smaller than the contribution from $\text{Re}\Sigma_{hL}^{(2)}$ at low electron density. The analogous calculation for Z_L with $\text{Re}\Sigma_{Lh}^{(2)}$ and $\text{Re}\Sigma_{LL}^{(2)}$ yields only $Z_L^{-1} \sim 1 + \lambda^2$ in 3D and $Z_L^{-1} \sim 1 + f_0^2$ in 2D (does not contain a large logarithm).

Correspondingly for the effective mass of a heavy particle according to [11.20, 12.27, 12.28] we have:

$$\frac{m_h}{m_h^*} = Z_h \left(1 + \frac{\partial \text{Re}\Sigma_{hL}^{(2)}(\epsilon_h(\vec{q}) - \mu, \vec{q})}{\partial \epsilon_h(\vec{q})} \Big|_{\epsilon_h(q) \rightarrow \mu} \right), \quad (12.3.39)$$

where the second contribution in brackets corresponds to the momentum dependence of the self-energy Σ_{hL} .

Therefore as usual the Z-factor contributes to the enhancement of a heavy mass:

$$\frac{m_h^*}{m_h} \sim Z_h^{-1} \sim \left(1 + 2\lambda^2 \ln \frac{m_h}{m_L} \right) \text{ in 3D} \quad (12.3.40)$$

Analogous calculations for Z-factor contribution to the light mass yields only

$$\frac{m_L^*}{m_L} \sim Z_L^{-1} \sim 1 + \lambda^2 \text{ in 3D} \quad (12.3.41)$$

If the effective parameter $2\lambda^2 \ln(m_h/m_L) > 1$ we are in the situation of strong electron polaron effect (strong EPE). To obtain the correct polaron exponent in this region of parameters diagrammatically, we should sum up at least the so-called maximally crossed diagrams for $\text{Re}\Sigma_{hL}$ [12.30]. But this exponent can be also evaluated in a different manner, based on the non-adiabatic part of the many particle wave-function [12.18] which describes the heavy particle dressed in a cloud of virtual electron – hole pairs of light particles. This yields:

$$\frac{m_h^*}{m_h} \sim Z_h^{-1} = \left(\frac{m_h}{m_L} \right)^{\frac{b}{(1-b)}}, \quad (12.3.42)$$

where $b = 2\lambda^2$ in 3D and $b = 2f_0^2$ in 2D.

For $b = 1/2$ or equivalently for $\lambda = 1/2$ in 3D or $f_0 = 1/2$ in 2D (as for the coupling constant for screened Coulomb interaction in 3D and 2D electron plasma in the RPA-theory - see preceding section 12.2 of this Chapter), we are in the so-called unitary limit. In this limit according to [12.18] the polaron exponent:

$$\frac{b}{(1-b)} = 1, \quad (12.3.43)$$

and hence:

$$\frac{m_h^*}{m_h} = \frac{m_h}{m_L} \quad (12.3.44)$$

or equivalently:

$$\frac{m_h^*}{m_L} = \left(\frac{m_h}{m_L} \right)^2. \quad (12.3.45)$$

Thus starting from the ratio between the bare masses $m_h/m_L \sim 10$ (obtained, for instance, in LDA-approximation [12.31]) we finish in the unitary limit with $m_h^*/m_L \sim 100$ (due to many-body electron-polaron effect), which is a typical ratio for uranium-based heavy-fermion systems [12.32-12.36].

12.3.5. Other mechanisms of heavy mass enhancement

We note that rigorously speaking (see (12.3.39)) the momentum dependence of $\text{Re}\Sigma_{hL}^{(2)}(\epsilon_h(\vec{q}) - \mu, \vec{q})$ is also very important for the evaluation of the effective mass. Preliminary estimates of Prokof'ev, Kagan (see also [12.4] and [11.34]) show that in the zeroth approximation in m_L/m_h in 3D case close to the Fermi-surface (for $\epsilon_h(\vec{q}) - \mu = (q^2 - p_{Fh}^2)/2m_h \rightarrow 0$ and $q \rightarrow p_{Fh}$):

$$\text{Re}\Sigma_{hL}^{(2)}(\epsilon_h(\vec{q}) - \mu, \vec{q}) \approx 2 \left(\frac{4\pi a_{hL}}{m_L} \right)^2 \int \frac{d^3 \vec{p}}{(2\pi)^3} \Pi_{LL}(0, \vec{p}) n_h^F(\vec{p} - \vec{q}), \quad (12.3.46)$$

where (see also (11.3.4))

$$\Pi_{LL}(0, \vec{p}) = \int \frac{d^3 \vec{p}'}{(2\pi)^3} \frac{[n_L^F(\epsilon_{p'+p} - \mu) - n_L^F(\epsilon_{p'} - \mu)]}{\epsilon_L(\vec{p}') - \epsilon_L(\vec{p}' + \vec{p})} \quad (12.3.47)$$

is a static polarization operator for light particles. Having in mind that $|\vec{p} - \vec{q}| < p_{Fh}$ and $q \approx p_{Fh}$ we can see that $\vec{p} \rightarrow 0$ and use the asymptotic form for $\Pi_{LL}(0, \vec{p})$ at small $p \ll p_{FL}$ (if the densities of heavy and light bands are not very different and $p_{FL} \sim p_{Fh}$):

$$\lim_{p \rightarrow 0} \Pi_{LL}(0, \vec{p}) = N_L^{3D}(0) \left[1 - \frac{p^2}{12 p_{FL}^2} \right], \quad (12.3.48)$$

where $N^{3D}_L(0) = m_L p_{FL}/2\pi^2$ is the density of states for light electrons in 3D. The substitution of $\lim_{p \rightarrow 0} \Pi_{LL}(0, \vec{p})$ from (12.3.48) to (12.3.46) yields:

$$\text{Re}\Sigma_{hL}^{(2)}(\epsilon_h(\vec{q}) - \mu, \vec{q}) \approx \text{Re}\Sigma_{hL}^{(2)}(0, p_{Fh}) - \frac{(q^2 - p_{Fh}^2)}{2m_h} \frac{\lambda^2}{9} \frac{m_h n_h}{m_L n_L}, \quad (12.3.49)$$

where $\lambda = 2a p_F/\pi$ is a 3D gas parameter, $n_h = p_{Fh}^3/3\pi^2$, $n_L = p_{FL}^3/3\pi^2$ are the densities of heavy and light bands.

The first term in (12.3.49) describes $\text{Re}\Sigma_{hL}^{(2)}(\epsilon_h(\vec{q}) - \mu, \vec{q})$ on the Fermi-surface (for $\epsilon_h(q) - \mu = 0$ and $q = p_{Fh}$). It reads:

$$\text{Re}\Sigma_{hL}^{(2)}(0, p_F) \approx \frac{4\lambda^2}{3} \frac{n_h}{n_L} \epsilon_{FL} \left(1 - \frac{2p_{Fh}^2}{15p_{FL}^2} \right) > 0 \text{ for } p_{FL} \sim p_{Fh} \quad (12.3.50)$$

It is renormalization of the effective chemical potential of the heavy band in the second order of the gas parameter due to the interaction of light and heavy particles.

We note that according to [11.19, 11.20] the renormalized heavy-particle spectrum is given by:

$$\epsilon_h^*(q) - \mu = \left(\frac{q^2}{2m_h} - \mu_h^{\text{eff}} \right) + \frac{2\pi}{m_L} n_L(\mu) a_{hL} + \text{Re}\Sigma_{hL}^{(2)}(\epsilon_h(\vec{q}) - \mu, \vec{q}) = \frac{(q^2 - p_{Fh}^2)}{2m_h^*}, \quad (12.3.51)$$

where the scattering length $a_{hL} \approx d$, an effective chemical potential $\mu_h^{\text{eff}} = \mu_h + W_h/2 + \epsilon_0$ is counted from the bottom of a heavy band, and the Hartree-Fock term $\frac{2\pi}{m_L} n_L(\mu) a_{hL}$ represents the contribution to the self-energy $\text{Re}\Sigma_{hL}^{(1)}$ in the first-order in the gas parameter. From (12.3.51) collecting the terms proportional to $\epsilon_h(\vec{q}) - \mu = (q^2 - p_{Fh}^2)/2m_h$ we obtain:

$$\frac{(q^2 - p_{Fh}^2)}{2m_h^*} = [\epsilon_h(q) - \mu] \left(1 - \frac{\lambda^2}{9} \frac{m_h n_h}{m_L n_L} \right). \quad (12.3.52)$$

Correspondingly, the effective mass of a heavy particle is given by:

$$\frac{m_h}{m_h^*} = 1 + \frac{\partial \text{Re}\Sigma_{hL}^{(2)}(\epsilon_h(q) - \mu, q)}{\partial(\epsilon_h(q) - \mu)} \bigg|_{\epsilon_h(q) \rightarrow \mu} = 1 - \frac{\lambda^2}{9} \frac{m_h n_h}{m_L n_L}. \quad (12.3.53)$$

As a result we obtain much more dramatic (linear in m_h/m_L) enhancement of m_h^* than in EPE (which yields only logarithmic in m_h/m_L enhancement $m_h/m_h^* \approx 1 - 2\lambda^2 \ln(m_h/m_L)$ due to the Z-factor of a heavy particle). For $m_h/m_L \sim 10$ the contribution to m_h^* in (12.3.53) becomes larger than the contribution to Z-factor in (12.3.40) for a large density mismatch $n_h \geq 5n_L$ between the heavy and light band. In general in the second order of the gas parameter in 3D:

$$\frac{m_h}{m_h^*} = 1 + \frac{\lambda^2}{9} \frac{m_h n_h}{m_L n_L} + 2\lambda^2 \ln \frac{m_h}{m_L} \quad (12.3.54)$$

We note that the contribution to m_h^*/m_h from $\text{Re}\Sigma_{hh}^{(2)}(\epsilon_h(q) - \mu, \vec{q})$ associated with the “heavy-heavy” interaction is small in comparison with the contribution to m_h^* from $\text{Re}\Sigma_{hL}^{(2)}$ (which is associated with “heavy-light” interaction) due to the smallness of the ratio between the bare

masses: $m_L/m_h \ll 1$. We can now collect the terms which do not depend upon $\epsilon_h(q) - \mu$ in (12.3.51). This gives the effective chemical potential of heavy electrons:

$$\mu_h^{\text{eff}} = \frac{p_{Fh}^2}{2m_h} + \frac{2\pi}{m_L} n_L(\mu) a_{hL} + \text{Re} \Sigma_{hL}^{(2)}(0, p_{Fh}) \quad (12.3.55)$$

We note that the contributions to μ_h^{eff} from the Hartree-Fock term $\frac{2\pi}{m_L} n_L(\mu) a_{hL}$ of heavy electrons and from $\text{Re} \Sigma_{hh}^{(2)}(0, p_{Fh})$ (which is connected with “heavy-heavy” interactions) are small in comparison with “heavy-light” contributions due to the smallness of the ratio between the bare masses: $m_L/m_h \ll 1$.

2D situation

In 2D the static polarization operator for light particles is (see [12.4, 11.34, 12.55]):

$$\Pi_{LL}(0, \vec{p}) = \frac{m_L}{2\pi} \left[1 - \text{Re} \sqrt{1 - \frac{4p_{FL}^2}{p^2}} \right], \quad (12.3.56)$$

and hence for $p < 2p_{FL}$: $\Pi_{LL}(0, \vec{p}) = \frac{m_L}{2\pi}$ - does not contain any dependence on p^2 in contrast to the 3D case. Thus EPE in 2D is a dominant mechanism of the heavy mass enhancement and in general in the second order of the gas parameter $\frac{m_h^*}{m_h} = 1 + 2f_0^2 \ln \frac{m_h}{m_L}$; $\frac{m_L^*}{m_L} \sim 1 + f_0^2$ in 2D.

In the end of this subsection we would like to note that the important role of the interband (“heavy”-“light”) Hubbard repulsion U_{hL} for the formation of a heavy mass $m^* \sim 100m_e$ in a two-band Hubbard model was also emphasized in [8.56] for the LiV_2O_4 HF compound.

The tendency towards phase-separation

We also note that for large density mismatch $n_h \gg n_L$ we could have a tendency towards phase-separation in a two-band model [12.4] in 3D. Namely if we evaluate the partial compressibility of the heavy component (the sound velocity of heavy particles squared):

$$\kappa_{hh}^{-1} \sim c_h^2 = \frac{n_h}{m_h} \left(\frac{\partial \mu_h^{\text{eff}}}{\partial n_h} \right) \quad (12.3.57)$$

we already see the tendency towards phase-separation $\kappa_{hh}^{-1} < 0$ (towards negative compressibility) in the strong coupling limit and low densities $\lambda^2 \frac{m_h p_{Fh}}{m_L p_{FL}} \geq 1$ in qualitative agreement with more phenomenological (mean-field type) variational approach [12.20].

The tendency towards phase-separation at low electron fillings also manifests itself for the asymmetric Hubbard model (where only interband Hubbard repulsion U_{hL} between heavy and light electrons is present and intraband Hubbard repulsions U_{hh} and U_{LL} are absent) in the limit of strong asymmetry $t_h < t_L$ [8.57] between heavy and light bandwidths.

In the end of this section we emphasize that the physics of EPE and evaluation of Z_h in [12.18] are to some extent connected with the well-known results of Nozieres et al., [12.19, 12.38] on infrared divergences in the description of the Brownian motion of a heavy particle in a Fermi-liquid and on the infrared divergences for the problem of X-ray photoemission from the

deep electron levels, as well as with the famous results of Anderson [12.39] on the orthogonality catastrophe for the 1D chain of N electrons under the addition of one impurity to the system.

Finally we mention a competing mechanism [12.40] proposed by Fulde for the explanation of the effective mass in praseodymium (Pr) and in some uranium-based molecules like $U(C_8H_8)_2$. Later on Fulde et al., [12.40] generalized this mechanism on some other uranium-based heavy-fermion (HF) compounds with localized and delocalized orbitals. This mechanism has a quantum-chemical nature and is based on the scattering of conductive electrons on localized orbitals as if on the two-level systems. The mass-enhancement is here governed by non-diagonal matrix elements of the Coulomb interaction which are not contained in the simple version of a two-band model (12.3.1). In this context we also mention [12.41] where the authors considered the mass-enhancement of conductivity electrons due to their scattering on local f -levels splitted by the crystalline field.

We note that de Haas van Alphen (dHvA) experiments [12.42] together with ARPES (angle-resolved photoemission spectroscopy) experiments [12.43] and thermodynamic measurements [12.33, 12.34, 12.44] are the main instruments to reconstruct the Fermi-surface for HF-compounds and to determine the effective mass (thus verifying the predictions of different theories regarding the mass enhancement in uranium-based HF-compounds).

12.3.6. Anomalous superconductivity in the two-band model with one narrow band.

For the sake of completeness let us consider briefly superconductivity problem in the same type of models [12.3] and namely in the two-band model with narrow band [12.4]. Let us concentrate on a 2D case where critical temperatures are higher already at low densities and consider the most typical case (see Fig. 12.8) $m_h > m_L$ and $p_{Fh} > p_{FL}$. We assume however that still the mismatch between the densities is not large enough to produce phase-separation. Note that in 2D case where only EPE is present the restrictions on a homogeneous state could be more mild than in a 3D case. At low densities $n_L d^2 < n_h d^2 \ll 1$ the maximal T_C corresponds to p-wave pairing and is governed by the enhanced Kohn – Luttinger mechanism of SC [11.4, 12.1, 12.3]. The general expression for the effective interaction U_{eff} of the heavy particles (for the irreducible bare vertex for the Cooper channel) in the first two orders in the gas-parameter reads:

$$U_{eff}(\vec{p}_h, \vec{p}_h') = T_{hh} + T_{hh}^2 \Pi_{hh}(0, \vec{q}_h = \vec{p}_h + \vec{p}_h') - 2T_{hL}^2 \Pi_{LL}(0, \vec{q}_h = \vec{p}_h - \vec{p}_h'), \quad (12.3.58)$$

where \vec{p}_h and \vec{p}_h' are incoming and outgoing momenta for the heavy particles in the Cooper channel, $|\vec{p}_h| = |\vec{p}_h'| = p_{Fh}$ and:

$$q_h^2 = 2p_{Fh}^2(1 - \cos \varphi); \quad \tilde{q}_h^2 = 2p_{Fh}^2(1 + \cos \varphi) \quad (12.3.59)$$

are transferred momentum squared (for q_h^2) and transferred momentum with an account of crossing squared (for \tilde{q}_h^2). These formulas are exactly analogous to (11.3.11), (11.3.16) but correspond to 2D case, φ is an angle between \vec{p}_h and \vec{p}_h' . Note that, as we discussed in Chapter 7, both transferred momenta $q_h \leq 2p_{Fh}$ and $\tilde{q}_h \leq 2p_{Fh}$ for superconductivity problem. The second term in (12.3.58) is connected with an exchange diagram (see Fig.11.2 and (11.3.10)) for heavy electrons while the third term is a static polarization operator (12.3.47).

In (12.3.58) for Π_{hh} and Π_{LL} we get:

$$\begin{aligned}\Pi_{hh}(0, \tilde{q}_h) &= Z_h^2 \frac{m_h^*}{2\pi} \left[1 - \text{Re} \sqrt{1 - \frac{4p_{Fh}^2}{\tilde{q}_h^2}} \right], \\ \Pi_{LL}(0, \tilde{q}_h) &= Z_L^2 \frac{m_L^*}{2\pi} \left[1 - \text{Re} \sqrt{1 - \frac{4p_{FL}^2}{\tilde{q}_h^2}} \right],\end{aligned}\quad (12.3.60)$$

where Z_h and m_h^* are Z- factor and effective mass of heavy particle, Z_L and m_L^* are Z- factor and effective mass of light particle, p_{Fh} and p_{FL} – are Fermi-momenta for heavy and light particles. Having in mind that $Z_L \sim m_L / m_L^* \sim (1-f_0^2)$, we can put $Z_L \sim 1$ and $m_L^* \sim m_L$ in all the forthcoming estimates. Finally in (12.3.58) for $p_{Fh} > p_{FL}$ the Kanamori T-matrices read in the strong coupling case in 2D:

$$T_{hh} = \frac{4\pi}{m_h^*} \frac{1}{\ln\left(\frac{1}{p_{Fh}^2 d^2}\right)} > 0, T_{hL} = \frac{4\pi}{m_L^*} \frac{1}{\ln\left(\frac{1}{p_{Fh}^2 d^2}\right)} > 0 \quad (12.3.61)$$

Having in mind that $\tilde{q}_h \leq 2p_{Fh}$ we get: $\Pi_{hh}(0, \tilde{q}_h) = Z_h^2 m_h^* / 2\pi$ – does not contain any dependence upon transferred momentum with crossing \tilde{q}_h .

In the same time $\Pi_{LL}(0, \tilde{q}_h)$ contains nontrivial dependence upon q_h for $p_{Fh} > p_{FL}$. We can say [12.1, 12.3, 12.4] that large 2D Kohn's anomaly becomes effective for SC – problem already in the second order of the gas-parameter and we have the pairing of heavy electrons via polarization of light electrons (see Fig. 12.12).

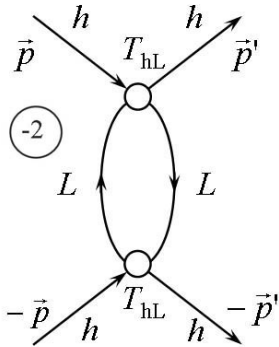


Fig. 12.12. The leading contribution to the effective interaction U_{eff} for the p-wave pairing of heavy particles via polarization of light particles. The open circles stand for the vacuum T-matrix T_{hL} .

Note that a standard s-wave pairing is suppressed in a two-band Hubbard model by short-range Hubbard repulsion which yields $T_{hh} > 0$ in the first-order contribution to U_{eff} in (12.3.58).

According to Landau-Thouless criterion [11.19] the maximal critical temperature in our model corresponds to triplet p-wave pairing (to pairing with magnetic quantum number $m = 1$ in 2D) and reads:

$$-U_{\text{eff}}^{m=1} N_{2D}^h(0) Z_h^2 \ln \frac{\mathcal{E}_{Fh}^*}{T_{C1}} = 1, \quad (12.3.62)$$

where $N_{2D}^h(0) = m_h^* / 2\pi$ is an effective 2D density of states for heavy electrons with effective heavy mass m_h^* ; $\mathcal{E}_{Fh}^* = p_{Fh}^2 / 2m_h^*$ - is renormalized Fermi-energy for heavy electrons; $U_{\text{eff}}^{m=1}$ is a p-wave harmonic of the effective interaction. It is given by:

$$U_{eff}^{m=1} = \int_0^{2\pi} U_{eff} [q(\cos \varphi)] \cos \varphi \frac{d\varphi}{2\pi} \quad (12.3.63)$$

It is shown in [12.1, 12.3, 12.4] that $U_{eff}^{m=1}$ depends upon relative occupation of the two bands p_{Fh}/p_{FL} and yields:

$$U_{eff}^{m=1} = N_{2D}^{L*}(0) \frac{(p_{Fh}/p_{FL} - 1)}{(p_{Fh}^2/p_{FL}^2)} T_{hL}^2 (-2) < 0. \quad (12.3.64)$$

Moreover it corresponds to attraction. In (12.3.64) $N_{2D}^{L*}(0) = m_L^*/2\pi$ is effective 2D density of states for light electrons. We can see that $U_{eff}^{m=1} \rightarrow 0$ for $p_{Fh}/p_{FL} \rightarrow 1$ and $p_{Fh}/p_{FL} \rightarrow \infty$. It is easy to show that $U_{eff}^{m=1}$ has rather large and broad maximum [12.1, 12.3, 12.4] for $p_{Fh} = 2p_{FL}$ or equivalently for $n_h = 4n_L$ (see Fig. 12.13). In maximum an effective interaction reads:

$$U_{eff}^{m=1} = -\frac{1}{2} N_{2D}^{L*}(0) \left(\frac{4\pi}{m_L^* \ln(1/p_{Fh}^2 d^2)} \right)^2. \quad (12.3.65)$$

Correspondingly Landau-Thouless criterion for superconducting temperature T_{C1} yields:

$$\frac{m_h^*}{m_L^*} Z_h^2 2f_0^2 \ln \frac{\varepsilon_{Fh}^*}{T_{C1}} = 1, \quad (12.3.66)$$

where $f_0 = \frac{1}{\ln(1/p_{Fh}^2 d^2)}$ is a 2D gas parameter. For $f_0^2 \ln \frac{m_h}{m_L} \leq 1$ EPE is weak and $m_h^* \approx m_h$.

Thus $Z_h \approx 1$, $\varepsilon_{Fh}^* \approx \varepsilon_{Fh}$ and Landau-Thouless criterion reads: $\left(\frac{m_h}{m_L} \right) 2f_0^2 \ln \frac{\varepsilon_{Fh}}{T_{c1}} = 1$. An effective

gas-parameter which enters the formula for T_{C1} for weak EPE is thus $f_0 \left(\frac{m_h}{m_L} \right)^{1/2}$. In weak-

coupling Born case for $U_{hh} \sim U_{hL} \sim U_{LL} < W_h < W_L$ the critical temperature $T_{C1} \sim \varepsilon_{Fh} \exp \left\{ -\frac{1}{2\tilde{f}_0^2} \right\}$

where $\tilde{f}_0 = \frac{\sqrt{m_L m_h} U_{hL}}{4\pi}$ is connected with interband Hubbard interaction U_{hL} and proportional to

geometric average of heavy and light masses $\sqrt{m_L m_h}$ (see [11.32, 12.3]). In opposite strong-

coupling case $U_{hL} > W_h > W_L$ the critical temperature $T_{C1} \sim \varepsilon_{Fh} \exp \left\{ -\frac{1}{2\tilde{f}_0^2} \right\}$ with effective gas-

parameter:

$$\tilde{f}_0 = \sqrt{\frac{m_h}{m_L}} \frac{1}{\ln \left(\frac{1}{p_{Fh}^2 d^2} \right)} \quad (12.3.67)$$

It is interesting to emphasize that in the unitary limit $f_0 \rightarrow 1/2$ the EPE yields for the heavy-mass enhancement $m_h^*/m_L \sim (m_h/m_L)^2$ and for Z -factor of heavy particle $Z_h \sim m_h/m_h^* \sim m_L/m_h$.

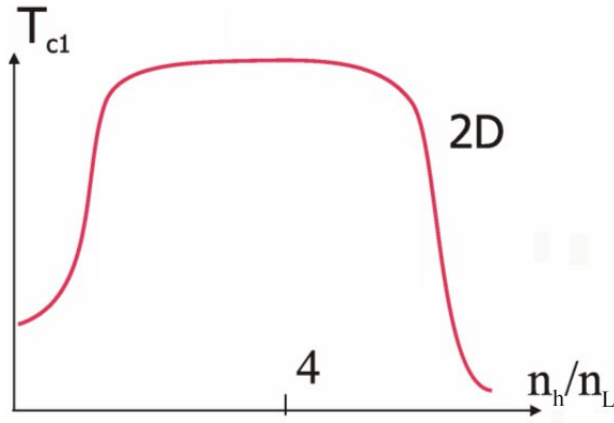


Fig. 12.13. Dependence of the critical temperature T_{C1} from the relative filling of heavy and light bands n_h/n_L in the two-band model with one narrow band. The maximum for T_{C1} corresponds to $n_h/n_L = 4$ in 2D.

If we assume that still $m_L^* \approx m_L$ even in unitary limit (for $f_0^2 = 1/4$) then we get for the combination $\frac{m_h^*}{m_L^*} Z_h^2$ in (12.3.66):

$$\frac{m_h^*}{m_L^*} Z_h^2 \sim \frac{m_h^*}{m_L^*} \left(\frac{m_h}{m_h^*} \right)^2 \sim \frac{m_h^2}{m_L^2} \frac{m_L^2}{m_h^2} \sim 1 \quad (12.3.68)$$

Thus for the critical temperature T_{C1} in the unitary limit $f_0 \rightarrow 1/2$ we can get:

$$T_{C1} \sim \varepsilon_{Fh}^* \exp \left\{ -\frac{1}{2f_0^2} \right\} \sim \varepsilon_{Fh}^* e^{-2}. \quad (12.3.69)$$

It means that for typical (for uranium-based HF compounds) values of $\varepsilon_{Fh}^* \sim (30 \div 50)$ K the critical temperatures are in the range of 5K already at low density which is quite reasonable.

Note that in a phase-separated state we have the droplets (clusters) with the density-ratio n_h/n_L larger or smaller than the density ratio in a homogeneous state [12.4]. For example in a fully phase-separated state we have two large clusters (1,2) with $n_{h1} > n_h > n_{h2}$ (that is so-called Maxwell construction [12.46] typical for phase-separated systems and first-order phase transitions). Thus the expression (12.3.64) for the critical temperature T_{C1} as a function of relative occupation is valid for both clusters but with local values of $(p_{Fh}/p_{FL})_1$ and $(p_{Fh}/p_{FL})_2$. Correspondingly the critical temperature will be different for these two clusters at least in zeroth approximation when we neglect the Josephson coupling [12.7, 12.19] or proximity effect [12.7, 12.19] between the neighboring clusters or droplets.

To finish the consideration of SC in the two-band model let us discuss briefly an effective interaction (irreducible bare vertex) for light electrons in the Cooper channel. It reads:

$$U_{eff}(\vec{p}_L, \vec{p}_L') = T_{LL} + T_{LL}^2 \Pi_{LL}(0, \vec{q}_L = \vec{p}_L + \vec{p}_L') - 2T_{hL}^2 \Pi_{hh}(0, \vec{q}_L = \vec{p}_L - \vec{p}_L'), \quad (12.3.70)$$

where incoming and outgoing momenta $|\vec{p}_L| = |\vec{p}_L'| = p_{FL}$ and transferred momenta $\vec{q}_L \leq 2p_{FL}; q_L \leq 2p_{FL}$ for SC-problem. The Kanamori T-matrix for light electrons T_{LL} in strong

coupling case reads $T_{LL} = \frac{4\pi}{m_L^* \ln(1/p_{Fh}^2 d^2)} > 0$. Using the expression for Π_{LL} and Π_{hh} :

$$\begin{aligned}\Pi_{LL}(0, \tilde{q}_L) &= Z_L^2 \frac{m_L^*}{2\pi} \left[1 - \text{Re} \sqrt{1 - \frac{4p_{FL}^2}{\tilde{q}_L^2}} \right], \\ \Pi_{hh}(0, \tilde{q}_L) &= Z_h^2 \frac{m_h^*}{2\pi} \left[1 - \text{Re} \sqrt{1 - \frac{4p_{Fh}^2}{q_L^2}} \right],\end{aligned}\quad (12.3.70)$$

and having in mind that $p_{Fh} > p_{FL}$ we get:

$$U_{\text{eff}}(\vec{p}_L, \vec{p}_L') \approx T_{LL} + T_{LL}^2 \frac{m_L^* Z_L^2}{2\pi} - 2 \frac{m_h^*}{2\pi} Z_h^2, \quad (12.3.71)$$

where we can put $Z_L \sim m_L / m_L^* \sim 1$.

Thus an effective interaction for light electrons does not contain any nontrivial dependence from \vec{q}_L and \tilde{q}_L and hence anomalous superconductivity with magnetic quantum number $m \neq 0$ is absent for light electrons in this approximation. Note that the standard s-wave pairing for light electrons is also suppressed by first order repulsive term $T_{LL} > 0$ in U_{eff} (12.3.71). However an inclusion of Moskalenko-Suhl-Geilihman term [12.47, 12.48], which describes rescattering of a Cooper pair between two bands and is given by:

$$K \sum_{pp'} (a_p^+ a_{-p}^+ b_p b_{-p'} + h.c.) \quad (12.3.72)$$

in the Hamiltonian of the two-band model (12.3.3) already in the case of infinitely small K makes the light band superconductive at the same temperature as the heavy one. This interesting fact was illustrated for standard s-wave pairing in [12.47] and for p-wave pairing in [12.45]. Thus T_{C1} in (12.3.62) is a mutual SC temperature in the two-band model with one narrow band [12.45]. Of course superconductive gaps for heavy and light bands open simultaneously at $T = T_{C1}$, but then “live their separate lives” for $T < T_{C1}$ (see [12.47]).

To conclude this section let us note that we discuss briefly the SC-instability which arises in the two-band model low electron density. The leading instability of the enhanced Kohn – Luttinger type [11.4, 12.1, 12.3] corresponds to triplet p-wave pairing of heavy electrons via polarization of light electrons. In 2D or quasi-2D case T_C can reach experimentally realistic values already at low densities for layered dichalcogenides CuS_2 , CuSe_2 and semimetallic superlattices InAs-GaSb , PbTe-SnTe with geometrically separated bands belonging to neighboring layers [12.3, 11.31]. Note that p-wave SC is widely discussed in 3D heavy-fermion systems like $\text{U}_{1-x}\text{Th}_x\text{Be}_{13}$ [11.10] and in layered ruthenates Sr_2RuO_4 [11.12, 12.49] with several pockets (bands) for conducting electrons [12.50]. Note also that when we increase the density of a heavy-band and go closer to half-filling ($n_h \rightarrow 1$) the d-wave superconductive pairing (as in UPt_3) becomes more beneficial in the framework of the spin-fluctuation theory in the heavy band [11.42, 11.43]. Different mechanisms of SC in HF-compounds including odd-frequency pairing introduced by Coleman, Miranda, Tsvelik are discussed in [12.51].

Note also that the multiband physics is important for some superconductive systems with conventional s-wave pairing including Nb [12.7], MgB_2 [11.14] and new superconductors based on FeAs-compounds like $\text{BaFe}_2(\text{As}_{1-x}\text{P}_x)_2$ [11.15]. For these compounds superconductive gaps in different bands are also open simultaneously at the same critical temperature due to Suhl-Moskalenko-Geilihman theory. All of them are very important for technical applications and energetics.

Note that the two-band Hubbard model discussed in this section is applicable also for degenerate case when there are two orbitals belonging to the same atom (when one atom is a source of electrons of two sorts) In the two-band degenerate Hubbard model $U = U_{hh} = U_{LL} = U_{hL} + 2J_H$ (where J_H is Hund’s coupling) [12.52]. Close to half-filling this model becomes

equivalent to the t - J orbital model [12.53] and contains for $J < t$ and at optimal doping the SC d -wave pairing [12.53] governed by superexchange interaction between the different orbitals of AFM-type ($J > 0$) with $J \sim t^2/U \sim 300$ K for not very different values of t_h and t_L . The physics of the t - J model will be described in detail in Chapter 13.

Reference to Chapter 12

- 12.1. M. Yu. Kagan, A. V. Chubukov, JETP Lett., 50, 483-486 (1989).
- 12.2. M. A. Baranov, D.V. Efremov, M. Yu. Kagan, Physica C: Supercond., 218, 75-81 (1993).
- 12.3. M. Yu. Kagan, Phys. Lett. A 152, 303-305 (1991).
- 12.4. M. Yu. Kagan, V. V. Val'kov, Sov. Phys. Low Temp. Special issue dedicated to 100th anniversary of Prof. D. Schoenberg, 37, 84-99 (2011) and also in "A Lifetime in Magnetism and Superconductivity: A Tribute to Professor David Schoenberg", Cambridge Scientific Publishers (2011).
- 12.5. G. Frossati, S. A. J. Wieggers, T. Tata, R. Jochemsen, P. G. van de Haar, L. P. Roobol, Czech. Jour. of Physics 40, 909-926 (1990); S.A.J. Wieggers, T. Hata, P.G. Van de Haar, L.P. Roobol, C.M.C.M. Van Woerkens, R. Jochemsen, G. Frossati, Physica B: Cond. Matt., 165-166, 733-734 (1990); L.P. Roobol, R. Jochemsen, C.M.C.M. van Woerkens, T. Hata, S.A.J. Wieggers, G. Frossati, Physica B: Cond. Matt., 165-166, 639-640 (1990).
- 12.6. G. Frossati, K. S. Bedell, S. A. J. Wieggers, G. A. Vermeulen, Phys. Rev. Lett. 57, 1032-1035 (1986).
- 12.7. M. Tinkham, Introduction to Superconductivity, McGraw-Hill, New York, 1975. P.G. de Gennes Superconductivity in Metals and Alloys, W. A. Benjamin Inc., New York, 1966
- 12.8. A.A. Abrikosov, L. P. Gor'kov, JETP 124, 1243 (1961).
- 12.9. K. Scharnberg, R. A. Klemm, Phys. Rev. B 22, 5233-5244 (1980); R. A. Klemm, K. Scharnberg, Phys. Rev. B 24, 6361-6382 (1981).
- 12.10. A.M. Clogston, Phys. Rev. Lett. 9, 266-267 (1962).
- 12.11. A.A. Abrikosov, Foundations of the theory of metals, Nauka, Moscow, 1987 (in Russian). C. Kittel, Introduction to Solid State Physics, 6-th Edition, New York 1986
- 12.12. N.V. Zavaritskii, Bull. Russ. Acad. of Sci., 78, 665 (1951) (in Russian).
- 12.13. T. Ando, A. B. Fowler, F. Stern, Rev. Mod. Phys. 54, 437-672 (1982).
- 12.14. C.T. Rieck, K. Scharnberg, R.A. Klemm, Physica C: Supercond., 170, 195-210 (1990).
- 12.15. Z. Tesaović, B. I. Halperin, Phys. Rev. B 36, 4888-4901 (1987).
- 12.16. H. Keitler, N. Grewe, in Valence Fluctuations in Solids, ed. by L. M. Falicov, North Holland Publishing Co., New York, USA, 1981.
- 12.17. D.M. Newns, N. Read, Adv. in Phys., 36, 799-849 (1987).
- 12.18. Yu. Kagan, N.V. Prokof'ev, JETP 66, 211 (1987); JETP 63, 1276 (1986).
- 12.19. G. Iche, P. Nozieres, Physica A, 91, 485-506 (1978).
- 12.20. A.O. Sboychakov, K. I. Kugel, A. L. Rakhmanov, Phys. Rev. B 76, 195113 (2007).
- 12.21. L. M. Falicov, J. C. Kimball, Phys. Rev. Lett. 22, 997-999 (1969).
- 12.22. G.D. Mahan, Many Particle Physics, Plenum, New York, 1981; J.W. Negele, H. Orland, Quantum Many Particle Systems, Addison-Wesley, Redwood City, CA, 1988
- 12.23. A. L. Fetter, J.D. Walecka, Quantum Theory of Many-Particle Systems, McGraw-Hill New York, 1971.
- 12.24. P. W. Anderson, Phys. Rev. Lett., 64, 1839-1841 (1990); Phys. Rev. Lett., 65, 2306 (1990); Phys. Rev. Lett., 66, 3226 (1991).
- 12.25. M. Yu. Kagan, V. V. Val'kov, P. Woelfle, Sov. Phys. Low. Temp, 37, 1046-1052 (2011).
- 12.26. J. R. Engelbrecht, M. Randeria, Phys. Rev. Lett., 65, 1032-1035 (1990); Phys. Rev. Lett., 66, 3225 (1991); Phys. Rev. B 45, 12419 (1992).
- 12.27. V.M. Galitskii, A.B. Migdal, JETP 7, 86 (1958).
- 12.28. D. Pines, P. Nozieres, Theory of Quantum Liquids, vol 1, W.A. Benjamin New York, 1966.

- 12.29. L.D. Landau, JETP 3, 920 (1957); JETP 5, 101 (1957).
- 12.30. P.Nozieres, Lectures in College de France (unpublished).
- 12.31. W. Kohn, L. J. Sham, Phys. Rev A, 140, 1133 (1965).
- 12.32. P. A. Lee, T. M. Rice, J. W. Serene, L. J. Sham, J. W. Wilkins, Comments on Condensed Matter Physics 12, 99 (1986).
- 12.33. G. R. Stewart, Rev. Mod. Phys., 56, 755–787 (1984).
- 12.34. H. R. Ott, Progr. in Low Temp. Phys., 11, 215-289 (1987).
- 12.35. N. Grewe, F. Steglich, in Handbook on the Physics and Chemistry of Rare Earths, vol. 14, ed. by K. A. Gachneider Jr, L. Eyring, North-Holland, Amsterdam, 1991.
- 12.36. P. Fulde, J. Keller, G. Zwicknagl, In Solid State Physics, Vol. 41, ed. by H. Ehrenreich, D. Turnbull, Academic, San Diego, 1988.
- 12.37. N. V. Prokof'ev, M. Yu. Kagan (unpublished).
- 12.38. P. Nozieres, C. T. de Dominicis, Phys. Rev., 178, 1097–1107 (1969).
- 12.39. P. W. Anderson, Phys. Rev. Lett. 18, 1049–1051 (1958); Phys. Rev., 164, 352–359 (1967).
- 12.40. R. M. White, P. Fulde, Phys. Rev. Lett., 47, 1540–1542 (1981); G. Zwicknagl, A. Yaresko, P. Fulde, Phys. Rev. B 65, 081103 (2002); Phys. Rev. B 68, 052508 (2003); M. Koga, W. Liu, M. Dolg, P. Fulde, Phys. Rev. B 57, 10648–10654 (1998).
- 12.41. Yu. Kagan, K.A. Kikoin, N.V. Prokof'ev, JETP Lett., 56, 219 (1992).
- 12.42. I.M. Lifshitz, A.M. Kosevich, JETP 2, 636 (1955); D. Shoenberg, Magnetic Oscillations in Metals, Cambridge University Press, 1984; L. Taillefer, G. G. Lonzarich, Phys. Rev. Lett., 60, 1570–1573 (1988); A. Wasserman, M. Springford, A. C. Hewson, J. Phys.: Condens. Matter 1, 2669 (1989).
- 12.43. T. Ito, H. Kumigishira, H.-D. Kim, T. Takahashi, N. Kimura, Y. Haga, E. Yamamoto, Y. Onuki, H. Harima, Phys. Rev. B 59, 8923–8929 (1999); A. J. Arko, J. J. Joyce, A. B. Andrews, J. D. Thompson, J. L. Smith, E. Moshopoulou, Z. Fisk, A. A. Menovsky, P. C. Canfield, C. G. Olson, Physica B: Condens. Matter 230-232, 16-21 (1997).
- 12.44. A. Berton, J. Chaussy, B. Cornut, J. Flouquet, J. Odin, J. Peyrard, F. Holtzberg, Phys. Rev. B 23, 3504–3513 (1981).
- 12.45. M. A. Baranov, M. Yu. Kagan, JETP 75, 165 (1992).
- 12.46. L. D. Landau, E. M. Lifshitz, Statistical Physics, Part I, Butterworth-Heinemann, Oxford, 1999.
- 12.47. H. Suhl, T.B. Matthias, L. R. Walker, Phys. Rev. Lett., 3, 552–554 (1959).
- 12.48. B. T. Geilikman, JETP 21, 796 (1965); Sov. Phys. Uspekhi 88, 327 (1966); *ibid* 109, 65 (1973).
- 12.49. F. Steglich, J. Aarts, C. D. Bredl, G. Cordier, F. R. de Boer, W. Lieke, U. Rauchschwalbe, in Superconductivity in d- and f-band Metals, Kernforschungszentrum, Karlsruhe, 1982.
- 12.50. M. Sigrist, K.Ueda, Rev. Mod. Phys., 63, 239–311 (1991).
- 12.51. P. Coleman, E. Miranda, A. Tsvelik, Phys. Rev. Lett., 70, 2960–2963 (1993); R. Flint, M. Dzero, P. Coleman, Nature Physics 4, 643–648 (2008) and reference therein; P. Coleman, , in Handbook of Magnetism and Advanced Magnetic Materials, vol. 1: Fundamentals and Theory, John Wiley and Sons, Hoboken, 2007.
- 12.52. K. I. Kugel, D. I. Khomskii, Sov. Phys. Uspekhi 136, 621 (1982).
- 12.53. S. Ishihara, J. Inoue, S. Maekawa, Phys. Rev. B 55, 8280–8286 (1997).
- 12.54. M. Yu. Kagan, T. M. Rice, J. Phys.: Condens. Matter 6, 3771 (1994).
- 12.55. A. M. Afans'ev, Yu. Kagan, JETP 43, 1456 (1962).
- 12.56. H. Kusunose, S. Yotsuhashi and K. Miyake, Phys. Rev. B, v.62, p. 4403 (2000)
- 12.57. P. Farkašovský, Phys. Rev. B, v.77, p. 085110 (2008)